Global Optimization Methods: Theoretical Aspects & Definitions

R.A. Van den Braembussche
von Karman Institute for Fluid Dynamics
Waterloose steenweg, 72
1640, Sint-Genesius-Rode

vdb@vki.ac.be

ABSTRACT

The first part of this lecture describes the basics of global optimizations systems with emphasis on those based on evolutionary strategies and the use of metafunctions to accelerate the convergence. The basic method is illustrated by the optimization of a 2D turbine blade.
It is followed by a description on how to extend the method to a ***multidisciplinary optimization****. The latter is illustrated by the optimization of a radial compressor impeller. It is shown how such a procedure can lead to innovative designs with high performance.*
*Further discussed and illustrated by an example are the procedures that may help to guarantee the performance over a wide operating range (****Multipoint Optimization****).*
The next chapter explains the notion of ***Robustness*** *and how to verify that small changes in operating conditions or design and manufacturing errors do not compromise the results.*
*The last part discusses the techniques that are available to handle designs that have more than one objective (****Multiobjective Optimization****).*

1. INTRODUCTION

The main goal when designing gasturbine components is to achieve light, compact and highly efficient systems while reducing the cost and the duration of the design cycle. The traditional trial-and-error process is now replaced by computerized design systems defining the optimum geometry for a required performance. They make use of a search technique to find the geometry that is optimum according to a performance prediction method, while respecting the design constraints.

Advanced design systems must allow full use of all the 3D geometrical features that may improve performance i.e. lean and sweep. Any limitation of the geometry is acceptable only if it is imposed by mechanical (stress), manufacturing or cost limitations. The optimal performance can only be guaranteed if all the real flow phenomena are taken into account i.e. if the performance predictions are made by 3D Navier-Stokes (NS) solvers. Any use of approximate (incorrect performance measuring systems) may lead to a false optimum. However those analysis tools require a large amount of computer effort, leading to excessive design cost. Hence methods must be developed that allow limiting the cost and time without compromising on the result.

The system must also provide realistic designs i.e. that satisfy the mechanical and geometrical constraints and guarantee the requested life time of the device. Satisfying all these objectives not only requires the use of acoustics, stress and heat transfer analysis methods (**multidisciplinary** optimization) but also requires a compromise to satisfy the conflicting objectives (**multiobjective** optimization). High performance must also be guaranteed over the whole operating range (**multipoint** optimization). A fast

and fully automated design system is required to achieve all this within a limited time and cost

Following describes optimization systems that reach these objectives in an efficient way i.e. with improved convergence, while taking into account the design and off-design operating conditions and constraints imposed by other disciplines. These methods are illustrated with different examples related to turbomachinery.

An optimization system consists of following components:

- A parameterized definition of the geometry
- An Objective Function (*OF*) expressing the design goals in a mathematical way.
- A performance prediction system, inclusive automatic grid generators, to providing the input for the *OF* for each newly proposed geometries
- A search mechanism that defines the design parameters that correspond to the best performance while satisfying the constraints (geometrical, mechanical, etc.)

2. SEARCH MECHANISMS

There are two main groups of search mechanisms:

The analytical ones, who calculate the required geometry changes in a deterministic way from the output of performance evaluations. A common one is the steepest descend method approaching the area of minimum *OF* by following the path with the largest negative gradient on the *OF* surface (Fig 1). This approach requires the calculation of the direction of the largest gradient of the *OF* and the step length. A comprehensive overview of this type of optimization techniques is given in the lecture of J. Peter [1].

Zero-order or stochastic search mechanisms require only function evaluations. They make a random or systematic sweep of the design space or use evolutionary theories such as Genetic Algorithms (GA) or Simulated Annealing (SA) to find the optimum parameter combination. Zero order methods may require more evaluations than gradient methods but the latter have more chances to get stuck in a local minimum. The present chapter concerns methods using zero order search mechanisms in combination with systems that allow reducing the computational effort by reducing the number of evaluations.

A systematic sweep of the design space, defining v values between the maximum and minimum limits of each of the n design variable requires v^n function evaluations. Fig.1 illustrates how such a systematic sweep, calculating the *OF* for 3 different values of X_1 and X_2, provides a very good estimation of where the optimum is located with only 9 function evaluations. This method is a valid alternative for analytical search methods for small values of n. However it requires more than 14. 10^6 evaluations for n =15.

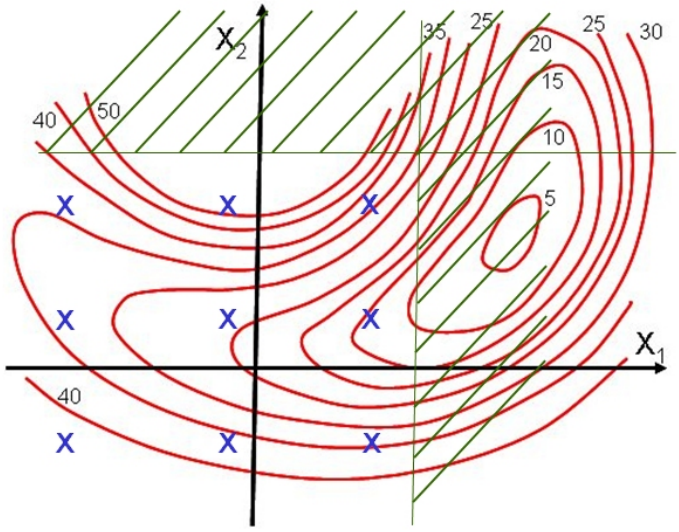

Fig. 1 Zero order sweep of the 2D design space

Evolutionary strategies such as GA and SA can accelerate the procedure by replacing the systematic sweep by a more intelligent selection of new geometries using in a stochastic way the information obtained during previous calculations. **Simulated Annealing** (SA) is derived from the annealing of solids [2]. At a given temperature, the state of the system varies randomly. The new state is immediately accepted if it has a lower energy level. If however the variation results in a higher level state, it is accepted only with a probability Pr that is function of the temperature.

$$\Pr = e^{\frac{E_{opt}-E_{act}}{T}}$$

As the temperature decreases, the probability of accepting a higher state becomes lower. In a simulated annealing algorithm, the design parameters characterize the state of the system whereas the objective function characterizes the energy level.

The method presented in present paper uses a **Genetic Algorithm** to find the optimum. This is a numerical technique, which simulates Darwin's evolutionary theory stating that the fitter survives [3]. According to this theory, an individual (geometry) with favorable genetic characteristics (design variables) will most likely produce better offsprings. Selecting them as parents increases the probability that individuals of the next generation will perform better than the previous one. The method has been developed by Prof. Ingo Rechenberg (Berlin, 1964) [4] who optimized an articulated plate with 5 degrees of freedom (design parameters) for minimum drag. Each articulation can take 53 values which results in a total number of 5^{51} = 345 025 251 possible geometries. The solution is quite obvious but difficult to find in a mathematical way.

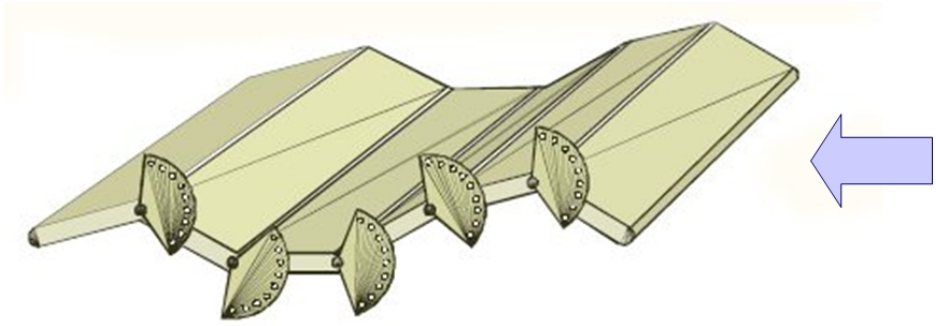

Fig. 2 Articulated plate of Ingo Rechenberg

In a standard binary coded GA, the real valued design parameters X_i, defining the geometry are jointly represented by a binary string.

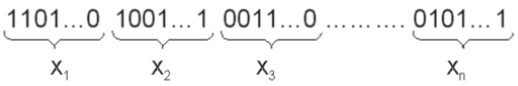

The substring length *l* defines the number of digits of a design parameters can take. *n* is the number of design parameters. Low values of the substring length decrease the optimization effort by limiting the possible number of solutions, but the GA may not be able to accurately locate the minimum because of a too low resolution.

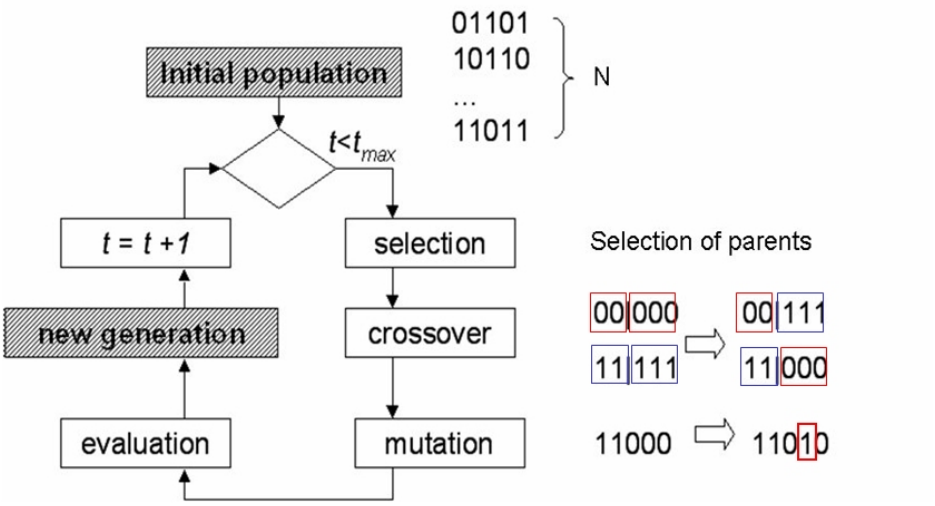

Fig. 3 Schematic of Genetic Algorithm

The operational principle of a standard GA is shown in Fig. 3. Pairs of individuals (parents) are selected from an initially random population of N geometries; each one is represented by a binary coded string of length *n.l*. Genetic material is subsequently exchanged between them (crossover), altered within the offspring (mutation), followed by an evaluation of each new individual. This process is repeated to create the N individuals of the next generation. The whole procedure is repeated for t_{max} generations and it is assumed that the best individual of the last generation is the optimum.

The GA software can be found on the Webb. The quality of the GA optimizer is measured by:

- the required computational effort i.e. the number of performance evaluations that are needed to find that optimum (GA efficiency).
- the value of the optimum (GA effectiveness).

The tuning of the GA parameters (N, *l, t*) to accelerated the convergence will be the subject of a second lecture [5]

The main issue of the GA is the selection scheme. One of the many selection schemes that have been proposed is the roulette (Fig. 4_{left}): a system in which the chance that an individual is selected increases proportional with 1/*OF*. This scheme favors the best individuals as parent. It is elitist and has larger chances to get stuck in a local optimum.

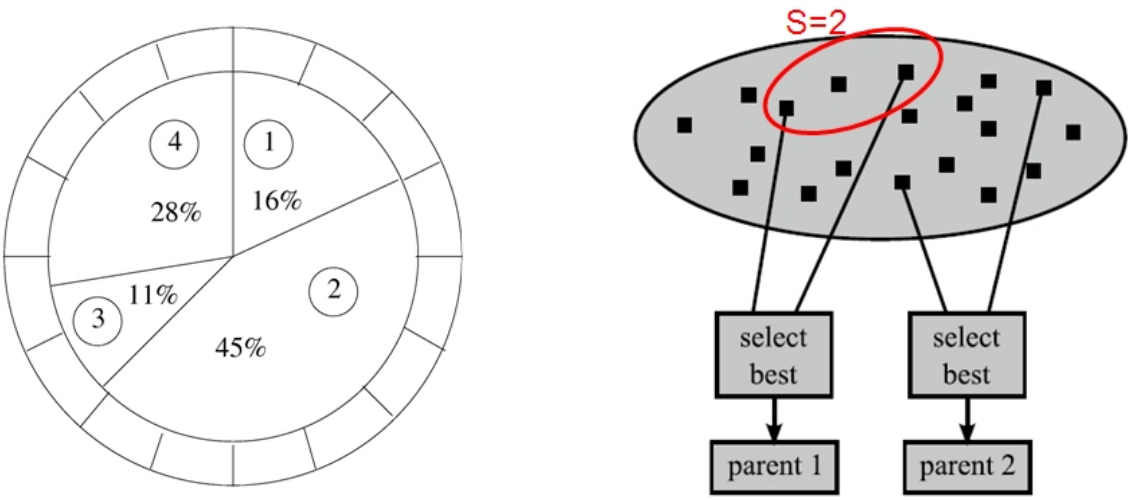

Fig. 4 Roulette (left) and tournament (right) selection

In the tournament selection (Fig. 4_{right}), S individuals are chosen randomly from the population and the individual with the lowest *OF* is selected as parent. The same process is repeated to find the second parent. The parameter S is called the tournament size and can take values between 1 and N. Larger values of *S* give more chances to the best samples to be selected and to create off-springs. It favors a rapid, but maybe premature, convergence to a local optimum. Too small values of S result in a more random selection of parents. Tests have shown that a standard value of S=2 gives the best results.

Zero order search methods, even supported by evolutionary theory, also require an excessive number of performance evaluations. This becomes prohibitive in cases with expensive performance evaluators. One way to speed up the convergence is by working on different levels of sophistication and by making better use of the knowledge, gained during previous designs, for subsequent ones. This is achieved by using fast but approximate prediction methods to find a near optimum geometry, which is then further verified and refined by the more sophisticated but also more expensive analyzer.

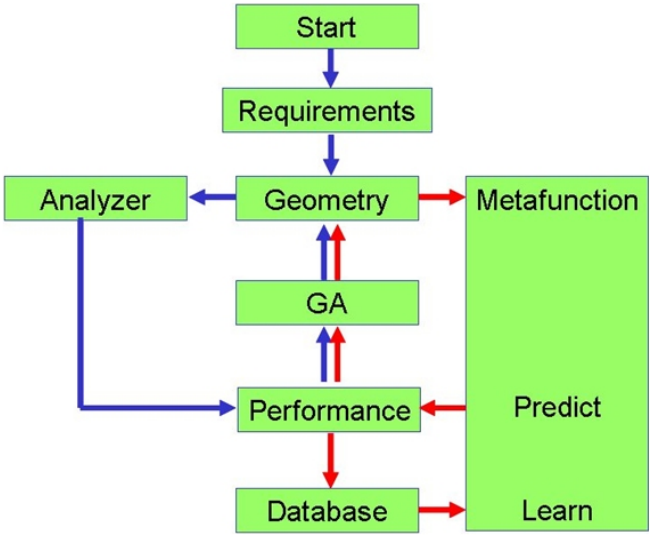

Fig. 5 Flowchart of optimization system

Such a system is illustrated by the flow chart on Fig. 5. [6]. The fast but less accurate optimization loop is indicated in red, the expensive but accurate one in bleu. The *OF* minimized by the GA is predicted by means of a Metafunction or surrogate model i.e. an interpolator using the information contained in the Database to correlate the performance to the geometry similar to what is done by a Navier-Stokes solver (NS). Surrogate models have the same input and output as the analysis method they replace. Once they have been trained on the data contained in the Database, they are very fast predictors and allow the evaluation of the *OF* of the many geometries, generated by the GA, with much less effort than a NS solver. Unfortunately the prediction is not always very accurate and the optimized geometry must be verified by means of a more accurate but time consuming NS solver. The results of this verification are added to the Database and a new optimization cycle is started. It is expected that a new learning on the extended Database will result in more accurate metafunction and that the result of the next GA optimization will be closer to the real optimum. The optimization cycle is stopped once the ANN performance is in agreement with the NS calculations i.e. once the GA optimization has been made with an accurate performance predictor.

The main advantage of this iterative procedure is the fact that, once the system is converged, there will be no discrepancy between the results of a Metafunction prediction and the one obtained by a Navier-Stokes calculation. Such an agreement is not guaranteed if a correlation or simplified solver (Euler or NS on course grid) are used because the inaccuracy is not released during the design process This might drive

the GA to a false optimum.

The accuracy of the Metafunction is a major factor defining the convergence of the system to the optimum. A GA optimization with an accurate Metafunction would result in a one step optimization, requiring only one extra performance analysis. The parameters influencing this convergence are discussed in a separate lecture [5].

The main purpose of the Database is to provide information about the relation between the geometry and the performance. The more general and complete this information, the more accurate may be the ANN and the closer the first optimum geometry, defined by the GA, will be to the real optimum. Hence a good Database may considerably speed up the convergence to the optimum.

Any approximating function can be used as metafunction. Popular ones are: Response surface, Artificial Neural Network (ANN), Radial Basis Functions (RBS), Kriging, etc. They will be explained in more detail in a later lecture [5] together with the way to define a more representative Database.

3. 2D TURBINE BLADE OPTIMIZATION

The convergence speed is also strongly influenced by the number of unknown that are needed to define the optimum geometry. Selecting parameters that have a direct relation to the performance, such as blade angles, pitch to chord ratio, etc. provide a more straightforward relation between geometry and performance. The corresponding ANN is simpler and more easily found. Hence less iterations may be needed to reach agreement with the NS predictions. Another important characteristic is the continuity of curvature of the blade contour because any discontinuous change in curvature may result in a local velocity peak.

3.1 Parameterization

A good geometry definition avoids the generation of unrealistic blades while having enough geometrical flexibility to represent a large number of blade types. The latter is very important because the best geometry can only be found if it can be generated by the system.

Table 1 2D turbine design parameters

$\beta_1$flow(o)	18.0
M_2^{is}	0.9
Re	5.8 10.5
γ=Cp/Cv	1.4
Tu(%)	4
Cax(m)	0.052
Pitch/Cax	1.0393
TE thick (m)	1.2 10.-3

	Imposed		After
	Min.	Max.	18 modif.
surface	5.2 10.-4	6.8 10.-4	5.36 10.-4
Imin(m4)	7.5 10.-9	1.2 10.-8	7.45 10.-9
Imax(m4)	1.25 10.-7	2.2 10.-7	1.28 10.-7
α_{Imax}	-50.00	-30.00	-37.50
$\beta_2$flow(o)	-57.80	57.80	-57.62
loss coef.(%)	0.0	0.0	1.9

Parameterization is illustrated by the single point optimization of a turbine blade with outlet Mach number .9. The design requirements are summarized in Table 1. They include the operating conditions (β_1 and M_2), flow characteristics (Re, γ, Tu (%) and geometrical constraints (C_{ax}, pitch and trailing edge thickness, maximum cross section area, minimum and maximum moment of inertia and direction), required performance (β_2 and losses).

The blade geometry (Fig. 8) is specified by four key points (LE, 2, 3, 5) linked by four curves. The points LE and 2 are linked by a Bézier curve defined by three additional points. The lasts ones are located in such a way to ensure continuity up to the third derivative at point 2 and continuity up to the first derivative in point 3. A Bézier Curve with three additional polygon points is used to define the pressure

side in the same way as the first part of the suction side. This curve is fully defined by β_{1blade}, R_{le}, L_4, α_{ps}, L_3 and the tangent to point 2. Using the same R_{le} and L_4 for both the suction and pressure side guarantees the continuity of the curvature radius at the leading edge. The trailing edge is defined by part of a circle whose radius R_{te} is specified by the Trailing edge thickness. The 2D blade geometry is thus fully defined by means of 15 parameters represented by G(n) : n=1,15

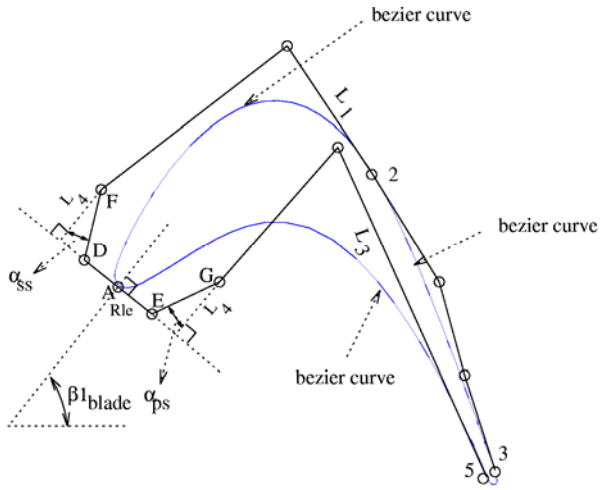

Fig. 8 Parameterized definition of 2D turbine blade

Fig. 9 shows 4 different types of turbine blades generated with this geometry model. For each blade one parameter is changed and its influence on the blade shape is shown. This figure demonstrates that the method is capable of representing the large variety of turbine blades encountered in industrial designs.

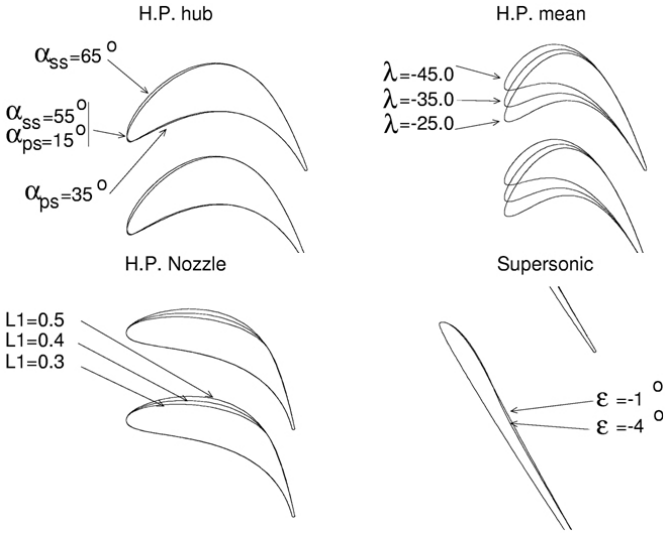

Fig. 9 Different parameterized blade geometries

3.2 Objective Function (OF)

The *OF* based on Navier-Stokes results predictions measures in how far the geometry satisfies the Aero-requirements and reaches the performance goals that have been set forward. The same *OF*, but based on ANN results, drives the GA towards the optimum geometry.

High efficiency however is not the only objective of an aerodynamic shape optimization. A good

design must respect the mechanical and manufacturing constraints. Some constraints must be satisfied without any compromise (i.e. maximum stress level) whereas others tolerate some margin (i.e. cost or weight) or can be corrected for after the design (adjusting the blade height to achieve the required mass flow).

A possible way to satisfy objectives and constraints is by defining a pseudo-*OF* by summing up the penalty terms that are increasing when the constraints are violated [7]. This does not guarantee that each individual constraint will be satisfied but contributes to a easier convergence to the constrained optimum.

Following lists some possible contributions to the pseudo *OF*.

$$OF_{2D} = w_{perf} \cdot P_{perf} + w_a \cdot P_{aeroBC} + w_M \cdot P_{Mach} + w_G \cdot P_{Geom} + w_S \cdot P_{Side}$$

$\boldsymbol{P_{perf}}$ is the penalty for non optimum performance i.e. low efficiency (η) or high losses.

$$P_{perf} = \max\left[\left|1-\eta\right|, 0.0\right]$$

$\boldsymbol{P_{AeroBC}}$ is the penalty for violating the aerodynamic boundary conditions. The purpose of this penalty is to enforce the design targets, such as the outlet flow angle (β_2) or the mass flow etc. These penalties start increasing when the actual value differs from the target value by more than a predefined tolerance. Following is a typical expression for mass flow penalty:

$$P_{mass} = w_i . \left[\max\left(\left|\dot{m}_{act} - \dot{m}_{req}\right| / \dot{m}_{req} - .02\ ,\ 0.\right)\right]^2$$

i.e. the penalty starts increasing when the error exceeds 2% of the required mass flow. The rate of increase is defined by w_i.

$\boldsymbol{P_{Mach}}$ is the penalty for non-optimum Mach number distribution. Analyzing the Mach number distribution may help to make a selection between blades that have nearly the same loss coefficient by decreasing the uncertainty due to transition predictions, or to favor Mach number distributions that are likely to perform better at off-design (see section 4. Multidisciplinary optimization).

$\boldsymbol{P_{Geom}}$ is the penalty for violating the geometrical constraints. These are the constraints that do not influence the mechanical integrity but restrict maximum length and camber or assure dimensional agreement with other components. Another reason to introduce geometrical constraints may be to favor geometrical features that are known to improve the design or off-design performance i.e. progressive change of curvature, some prescribed lean or sweep laws, limiting camber of the uncovered turbine suction side, etc .

$\boldsymbol{P_{Side}}$ is the penalty for violating any other constraint that might be imposed depending on the application i.e. weight, manufacturing and maintenance cost, etc

3.3 Results

The best blade of the initial database is used as starting geometry. The Mach distribution predicted by the NS and ANN are compared on Fig. 10a. The agreement is not perfect but the main features such as a shock at mid chord are predicted by the ANN.

Fig. 10b compares the value of the *OF* predicted by the ANN with the one predicted by the NS solver during the design process. The value of the *OF* computed by the approximate model decreases until iteration 13 after which only very small improvements are found. The value predicted by the NS solver shows large discrepancies between both predictions at iteration 2, 5 and 9. It indicates that during these first design iterations, the ANN predictions are not very accurate because the Database does not sufficiently cover the relevant design space. However this shortcoming is remediated by adding new

geometries to the Database. As these new blades are close to the desired operating point they provide very valuable information and the ANN becomes more and more accurate. This convergence to the same OF value illustrates the self learning capacity of the proposed procedure. Starting from iteration 13 the ANN predictions are very reliable. The whole procedure could have been stopped after 15 iterations but has been continued to verify the good convergence.

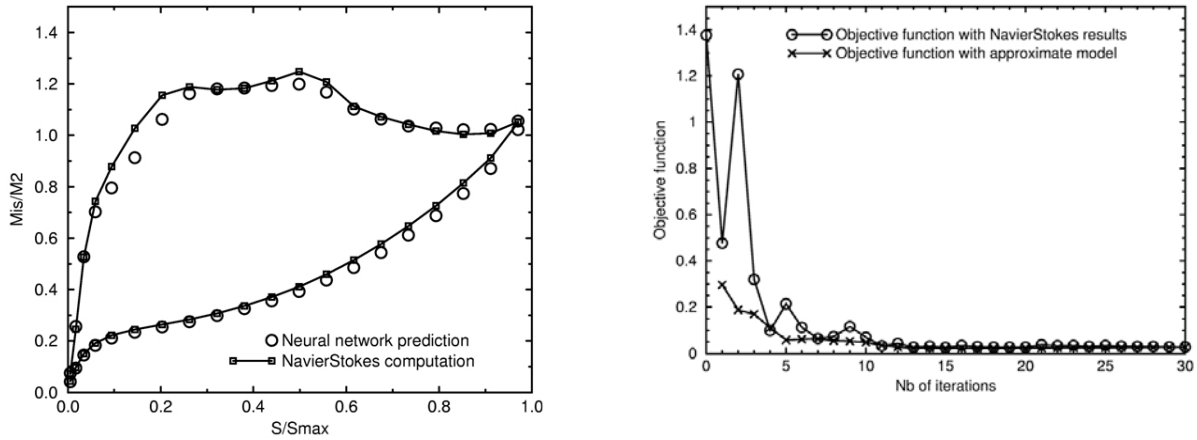

Fig. 10 Comparison of (a) Mach number distribution predicted by Navier-Stokes solve and ANN, trained on initial database and (b) between the ANN and the NS predicted *OF*

Figure 11 shows the variation of the Mach number distribution and blade shape during the design process. The small constant velocity region on the suction side close to the leading edge and the low velocity on the pressure side close to the leading edge indicate that the incidence angle on the initial blade is too large. After the first modification (one GA and NS verification), this incidence angle has been partially reduced by decreasing the stagger angle. The shock intensity is also smaller but the suction side Mach number distribution is still wavy. The shock has completely disappeared after 13 design iterations. The stagger angle has decreased in order to adapt the blade geometry to the prescribed inlet flow angle. The smooth shock free Mach number distribution is reflected in the low loss coefficient (Table 1).

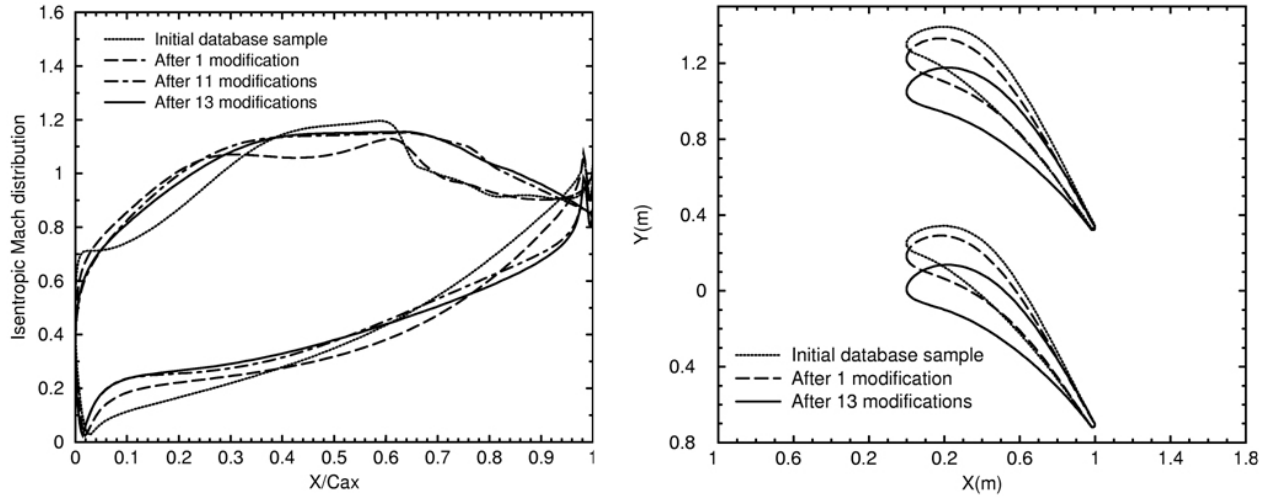

Fig. 11 Evolution of the Mach number distribution and geometry during optimization

4. MULTIDISCIPLINARY OPTIMIZATION.

Most mechanical constraints such as maximum stress and deformation have a direct impact on the turbomachinery integrity and must therefore be rigorously respected. Hence they cannot be imposed by a weak formulation as done for the geometrical constraints. Some of those constraints can easily be respected by a simple limitation of a design parameter. Bird ingestion resistance is often expressed by a minimum leading edge radius (R_{LE}) . Corrosion may define the minimum trailing edge radius (R_{TE}) and blade thickness ($B_{thickness}$). However most of the mechanically unacceptable geometries result from a combination of different parameters and cannot be avoided by reducing the feasible range of the individual design parameters. Hence, a large percentage of the design space will consist of geometries violating the constraint.

A possible approach is a verification of the mechanical constraints by a Finite Element Analysis (FEA) before starting the Aero analysis on every geometry proposed by the GA. This sequential analysis is very time consuming and is easily be replaced by a parallel analysis shown on Fig. 12. It is an extension of the flow chart shown in Fig. 5. The GA, searching for the optimum geometry, gets its input from the Finite Element stress Analysis (FEA) as well as from the NS flow analysis. The same type of extension could also be made for the constraints related to heat transfer, acoustics, weight limitations, etc.

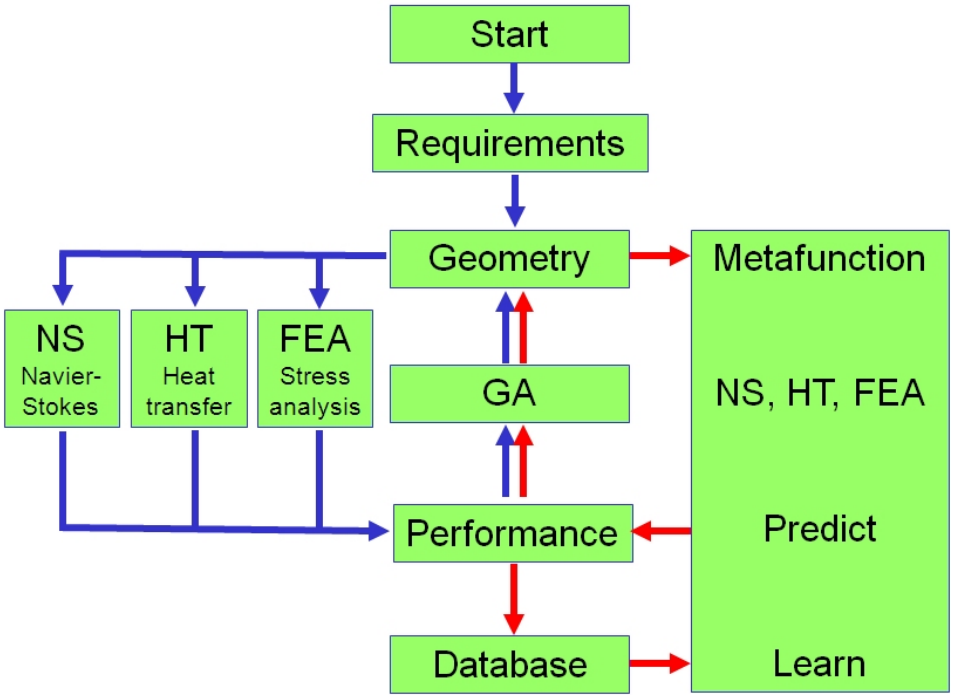

Fig.12 Multidisciplinary optimization flow chart

The main advantages of such an approach are:

- The existence of only one "master" geometry i.e. the one defined by the geometrical parameters used in the GA optimizer. This eliminates all possible approximations and errors when transmitting the geometry from one discipline to another.
- The existence of a global *OF* accounting for all disciplines. This allows a more direct convergence to the optimum geometry without iterations between the aerodynamically optimum geometry and the mechanically acceptable one.
- the possibility to do parallel calculations. The different analyses can be made in parallel if each discipline is independent i.e. if stress calculations do not need the pressure distribution on the vanes or flow calculations are not influenced by geometry deformations.

The computational effort increases proportional with the number of different analyses that are needed for the performance evaluation of the GA proposed geometries. It can be drastically reduced if one can eliminate the unfeasible geometries before any expensive flow analysis is started i.e. if, in analogy with the aero analysis, one can formulate an approximate prediction model for mechanical characteristics, heat transfer, etc. to drive the GA

The multidisciplinary optimization is illustrated by the design of a radial compressor impeller for a micro-gasturbine application with a diameter of 20 mm rotating at 500,000 rpm..

4.1 Geometry Definition

The 3D radial impeller is defined by the meridional contour at the hub and shroud (Fig 13), the camber line of the main and splitter blade (Fig 14), the thickness distribution normal to the camber line (Fig. 15) and the number of blades.

The hub and shroud meridional contours from the leading to the trailing edge are defined by third order Bézier curves (Fig 13). The coordinates of the control points are geometrical parameters that can be changed by the optimization program. Only 6 parameters are needed to define the meridional contour. Each of them has a limited range in which it can vary. The possible variations of the individual Bézier control points are shown by arrows in Fig. 13. The control point at the hub trailing edge is fixed by the prescribed outlet diameter and axial length. Most control points have only one degree of freedom because they are linked to other parameters in order to guarantee an axial inlet or radial outlet. The shroud leading edge diameter defines the variable impeller inlet height. Third order Bézier curves define also the inlet duct. Their control points are automatically adjusted to obtain a smooth link between the given radial inlet and impeller.

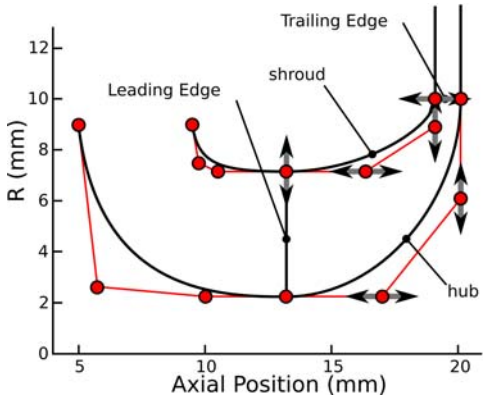

Fig. 13 Meridional contour defined by Bézier control points.

The blade camber lines at hub and shroud are defined by the distribution of the angle $\beta(u)$ between the meridional plane m and the blade camberline (Fig. 14). The β distributions at hub and shroud are defined by third order polynomials:

$$\beta(u) = \beta_0(1-u)^3 + 3\beta_1 u(1-u)^2 + 3\beta_2 u^2(1-u) + \beta_3 u^3$$

with u the non-dimensional meridional length ($u \in [0,1]$, 0 at the leading edge and 1 at the trailing edge). The camber line circumferential position θ (Fig. 14) is then defined by integration of:

$$R\,d\theta = dm \tan\beta$$

β_0 and β_3 are the blade angles at leading- and trailing edge. This definition is used for both the main- and splitter blade, at hub and shroud. The splitter trailing edge angles are the same as the full blade values at hub and shroud. This results in 14 design variables for the blade camber line definition.

The streamwise position of the splitter blade leading edge is also a design parameter. It is defined as a percentage of the main blade camber length and can vary between 20% and 35%.

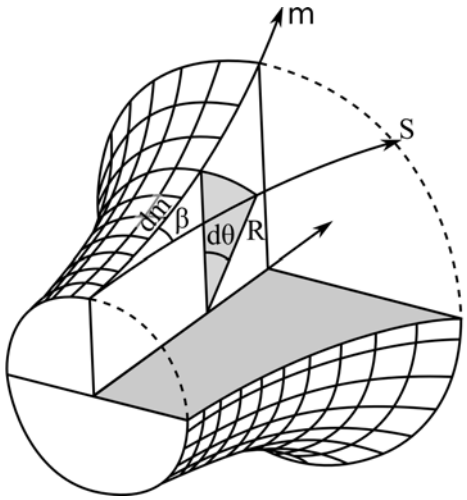

Fig. 14 Definition of the blade camber line by β angle.

The blade thickness distributions at hub and shroud are functions of two parameters: the thickness "LE" of the ellipse defining the leading edge and the trailing edge thickness "TE" (Fig. 15). The blade thickness is kept constant at the shroud (LE=TE=0.3 mm). The two parameters defining the blade thickness at the hub are design parameters and can vary between 0.3 to 0.6 mm. The same values are used for the main and splitter blade.

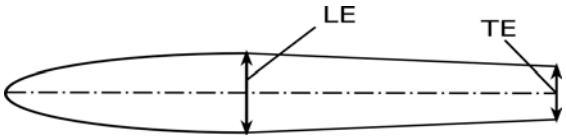

Fig. 15 Thickness distribution along the camber line of the blade (not to scale).

The number of blades could also be a design parameter to be optimized, but has been fixed to 7 for manufacturing reasons. This brings the total number of design parameters to 23.

4.2 Analysis programs

The TRAF3D Navier-Stokes solver [8] is used to predict the aerodynamic performance of the radial compressors. The computational domain starts at constant radius in the radial inlet (Fig. 13) and ends in the vaneless diffuser at $r/r_2 = 1.5$.

A structured H-grid with 2x216x48x52 or approximately 1,080,000 cells is used for all computations to guarantee a comparable accuracy for all the samples stored in the database. The total inlet temperature is 293°K and the total inlet pressure is 1.013E+5 Pa. The design mass flow is 20 g/s. The wall temperature of the impeller is fixed at 400º K, as found in a previous study on the heat transfer inside the entire micro gas turbine [9].

The commercial code SAMCEF [10] is used for the stress calculation. Quadratic tetrahedral elements are used as a compromise between element quality and automatic meshing. Similar grids with 250,000 nodes and 160,000 elements are used for all samples. The grid is refined in areas of stress concentrations.

The impeller tip speed of 523.6 m/s results in very high centrifugal stresses. Titanium TI-6AL-4V has been selected for its high yield stress over mass density ratio (σ_{yield}/ρ). The characteristics are: Elasticity modulus = 113.8E+9 Pa, Poisson modulus = .342 and mass density = 4.42E+3 kg/m^3.

A fillet radius of 0.25 mm is applied at the blade hub to limit the local stress concentrations. The unshrouded impeller has a tip clearance of 0.1 mm, which is 10% of the exit blade height. This is typical for these small impellers and one of the reasons for the moderate efficiencies.

4.3 Objective Function

The *OF* is the weighted sum of several penalties:

$$OF(\vec{G}) = w_{stress} \cdot P_{stress}(\vec{G}) + w_{\eta} \cdot P_{\eta}(\vec{G}) + w_{massflow} \cdot P_{massflow}(\vec{G}) + w_{Mach} \cdot P_{Mach}(\vec{G})$$

The first penalty concerns the mechanical stresses.

$$P_{stress} = \max\left[\frac{\sigma_{\max} - \sigma_{allowable}}{\sigma_{allowable}}, 0.0\right]$$

where σ_{max} is the maximum stress in the impeller. This penalty is zero when the stresses are below the allowable limit $\sigma_{allowable}$ and increases linearly when the von Mises stresses exceeding that value. This weak formulation of the constraints does not guarantee that they are fully respected. However, it has the advantage that all geometries that have been analyzed provide information that leads towards the optimum geometry.

The efficiency and Mass flow penalties are similar to the ones used for the 2D turbine. The penalty on the Mach number aims to favour Mach number distributions that are expected to be good at design point and remain good at off-design operation. It also has two contributions. The first one penalizes negative loading and is proportional to the area between the suction and pressure side when the pressure side Mach number is higher than the suction side one (Fig. 16).

$$P_{Mach} = \int_0^1 \max\left[M_{ps}(s) - M_{ss}(s), 0.0\right] \cdot ds$$

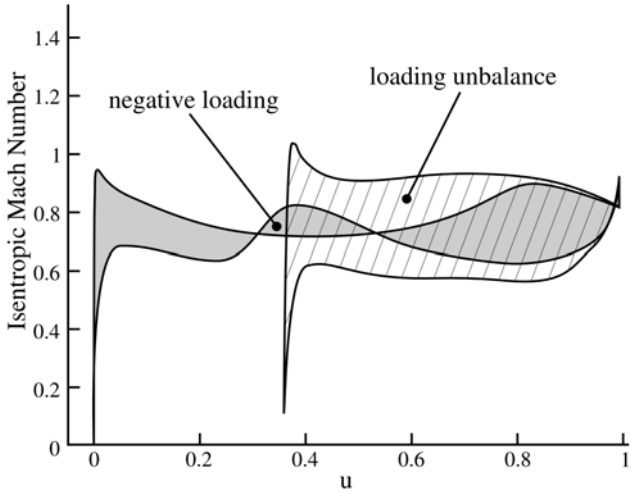

Fig. 16 Negative loading and loading unbalance in a compressor with splitter vanes.

The second Mach penalty increases with the loading unbalance between main blade and splitter blade. This penalty compares the area between the suction- and pressure side Mach number distribution of main blade A_{bl} and splitter blade A_{sp}, corrected for the difference in blade length (Fig. 16):

$$P_{loading\ unbalance} = \left(\frac{A_{bl} - A_{sp}}{A_{bl} + A_{sp}}\right)^2$$

The weight factors of the *OF* are determined based on the knowledge gained in previous optimizations. The values used in present design are such that an efficiency drop of 1% is as penalizing as an excess in stress limit of 6.668 MPa.

4.4 Results

The optimization starts from the outcome of a simple aerodynamic optimization without stress computation. It is called the "Baseline" impeller. Although this geometry has a good efficiency, it cannot be used because a mechanical stress analysis predicts von Mises stresses in excess of 750 MPa. It serves as a reference for further optimizations.

An initial database containing a total of 53 geometries is used at the start. 13 geometries out of the 64 initial ones defined by the DOE technique [5] could not be analyzed because of geometrical constraints (intersection of the main blade with the splitter blade). Two additional geometries have been added, namely the baseline geometry and the central case. The latter one is a geometry with all parameters at 50% of their range.

Fig. 17 shows the convergence history of the optimization. The "aero penalty", based on efficiency, Mach number and mass flow, the "stress penalty" and "total penalty", obtained from the Navier-Stokes and FEA calculations, are compared to the ones predicted by the ANN. One observes a decrease of the discrepancy between both prediction methods with iteration number. This is the consequence of an increasing number of samples in the database, resulting in a more accurate ANN.

Only 10 iterations are needed to obtain a very good agreement for the aero penalties. The ANN stress penalty is zero for every geometry proposed by the GA. However it takes more than 15 iterations before the FEA confirms that the proposed geometries satisfy the mechanical requirements.

The good agreement in both stress- and aero penalties, over the last 18 iterations, indicates that the ANN predictions are reliable. It means that the same optimum geometry would have been obtained if the GA optimization had been driven by the more sophisticated NS and FEA analyses. Hence no further improvement can be expected. The optimization procedure could already have been stopped after 35 iterations.

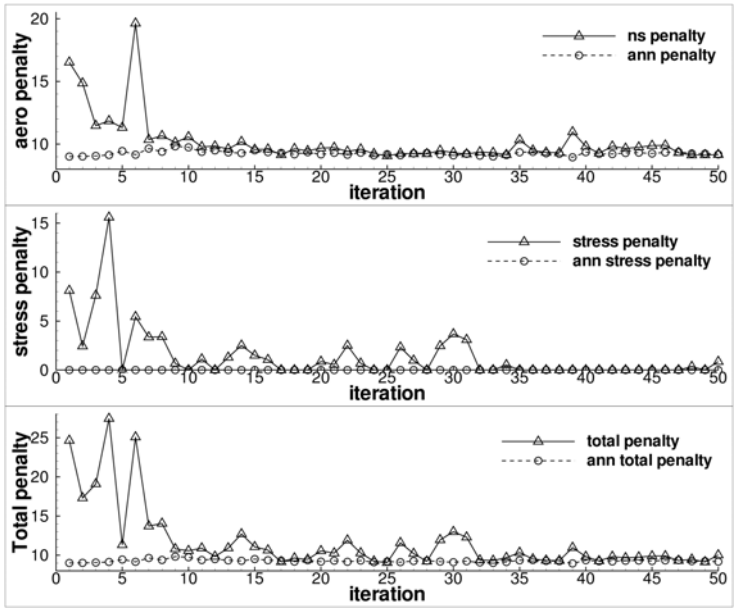

Fig. 17 Convergence history of the optimization.

The aero penalty is plotted versus the stress penalty in Fig. 18. The geometries created during the optimization process are all in the region of low penalties. Most of them outperform the geometries of the database. Only a few geometries of the optimization loop have penalties of the same order as the database samples. Those geometries are the ones created during the first 10 iterations where the ANN is still inaccurate.

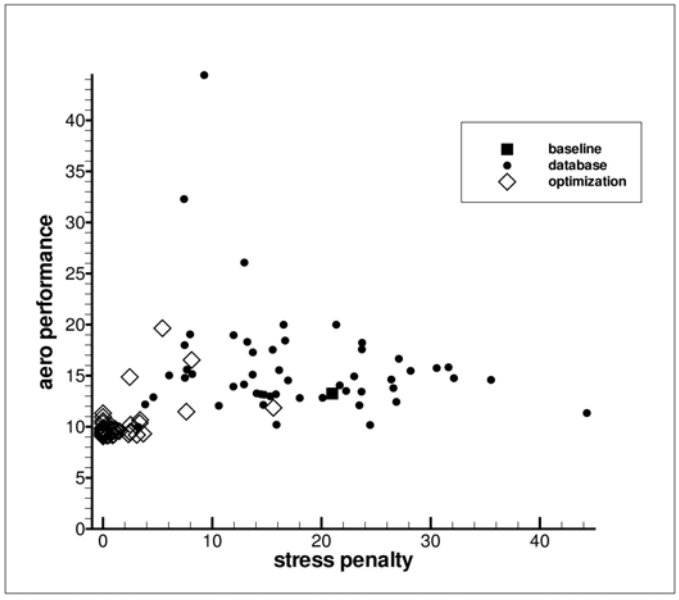

Fig. 18 Aero penalty versus stress penalty for baseline, database- and optimization geometries.

Fig. 19 is a zoom on the low penalty region of Fig. 18. A large number of geometries have zero stress penalties but with different aero penalty. The geometries corresponding to iteration 17, 49 and 25 have the lowest aero penalty.

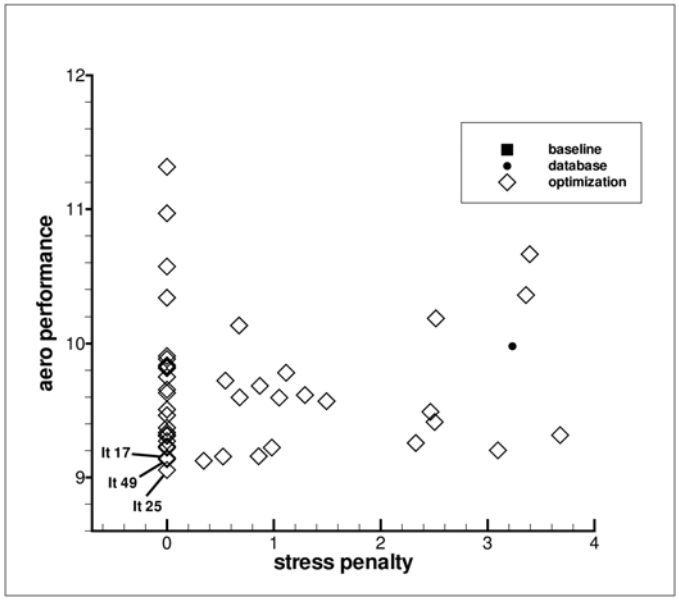

Fig. 19 Zoom on the low penalty region of Fig. 18.

From all geometries created during the optimization, iteration 25 performs best. It has a little lower efficiency than iteration 17 but less loading unbalance and the stresses are 33 MPa below the limit. In spite of its high efficiency the baseline impeller shows a high aero penalty because of a too high mass flow. The influence of the stress penalty on the optimization is clear by comparing the values of the baseline impeller with the ones of iteration 25. The reduction of the maximum stress level with 370 MPa is at the cost of a 2.3 % decrease of efficiency (21).

Figure 20 compares the von Mises stresses in the baseline geometry with the ones of iteration 25.

The drastic reduction in stress is the consequence of:

- the reduced blade height at the leading edge, resulting in lower centrifugal forces at the leading edge hub
- the increase of blade thickness at the hub
- the modified blade curvature resulting in less bending by centrifugal forces

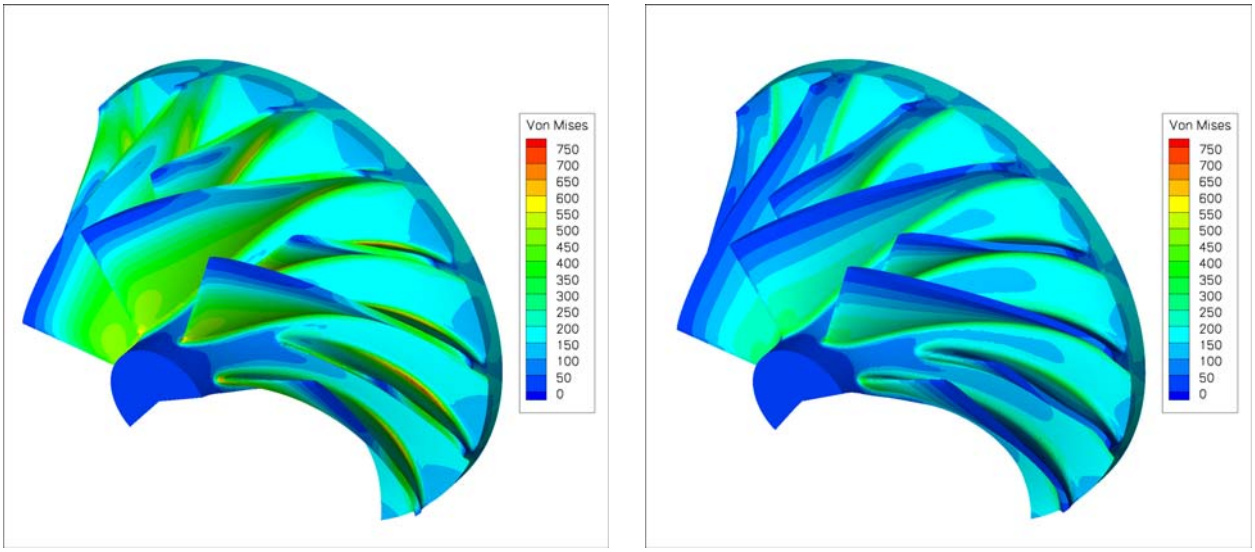

Fig. 20 von Mises stresses due to centrifugal loading in the baseline (left) and optimized (right) impeller.

The blade lean is defined as the angle between the blade leading edge and the meridional plane (positive in the direction of rotation). It is a result of the integration of the β distribution at hub and shroud, while limiting the rake at the outlet. Its impact on stress and efficiency is shown in Fig. 21. One observes a rather clear relation between lean and stress. It shows that the lowest stresses can be expected around -15.0º. Several geometries with good efficiency are found for lean angles between -40.0º to -5.0º. The drop in efficiency for lean angles above -5.0 º suggests that in present application the best impellers have some negative lean. This unexpected result is a major outcome of the optimization.

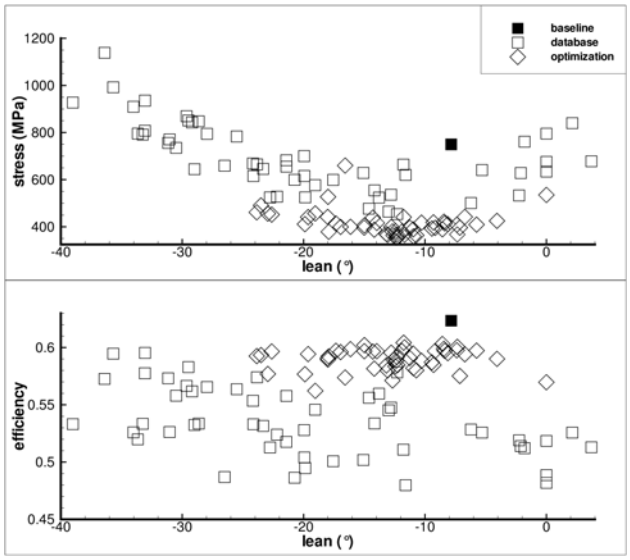

Fig. 21 Blade lean versus stress and efficiency for database and optimization geometries.

5. ROBUSTNESS

Robustness characteerizes the insensitivity of the performance to small changes in operating conditions or geometrical changes (manufacturing inaccuracies).

Small variations of incidence may trigger flow separation in turbomachinery components operating at the verge of separation (limited diffusion factor) and be at the origin of large performance variations. As will be demonstrated later this problem can be avoided by a multipoint optimization. Small changes in operating conditions or flow characteristics may result in large performance changes due to a large shift of the transition point. This can be avoided by adding penalties on the predicted Mach number distribution to account for the expected changes at off-design operation.

Small geometrical changes or manufacturing inaccuracies should not influence the performance. The results of the many geometries that have been analysed during the optimization process provide an indication of robustness. Figure 21 shows that a change in blade lean around the optimum value has almost no effect on stresses and efficiency. The design is robust in this respect.

Fig. 22 shows the stress and efficiency versus blade thickness at the leading edge for all geometries. Non-dimensional values 0 and 1 correspond to a blade thickness of respectively 0.3 and 0.6 mm. The database geometries are at 25% or 75% of the range suggest that the blade hub thickness does not have much impact on efficiency. Hence thicker blades are selected because it lowers the stresses. The figure also shows that thicker blades are more likely to have a lower stress than thin ones and that the stresses are not very sensitive to variations near the maximum thickness.

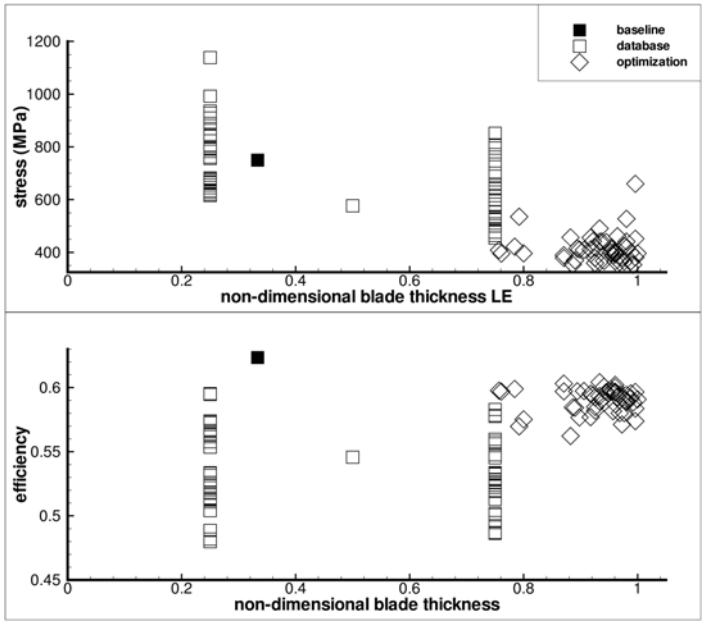

Fig. 22 Stress and efficiency versus blade thickness for database and optimization geometries.

6. MULTIPOINT OPTIMIZATION

Multipoint optimization aims for a design that performs well in more than one operating point. The simplest straight forward approach is to analyze every candidate geometry at the different operating conditions and to calculate a weighted value of the performance. This is not only expensive in terms of flow analysis but often compromised by practical problems.

When doing multipoint optimization one should make distinction between cases with varying inlet conditions or varying outlet conditions (back pressure). In the latter case one cannot a priori guarantee that

the proposed component can operate steadily at each point i.e. that the NS solver can provide a converged solution at the required operating conditions. In fact, it is not a priori known at what pressure ratio a compressor will surge because the change in mass flow with pressure ratio depends on the still unknown performance curve of the compressor. Less problems occur at the maximum mass flow side because any low back pressure provides a good idea of the choking or maximum mass flow and does not create stability problems.

The stability problem is less likely to occur for turbines. Operating with a favorable pressure gradient facilitates the convergence of the N.S. calculations and changing inlet angle of back pressure is less of a problem.

Variation of the inlet conditions is less risky in terms of calculation stability than change in outlet conditions.

Following describes an application where the off-design corresponds to a known variation of the inlet conditions and where the outlet conditions have less impact on the procedure. It is followed by a description of the procedure that has been put in place to do a multipoint optimization for compressors where the surge point prediction is a major issue.

6.1 Multipoint optimization of a Low Solidity Diffuser

Radial compressors with vaned diffusers provide high pressure recovery and efficiency but the operating range is limited by stall, at positive incidence, and diffuser throat choking, at negative incidence. Vaneless diffusers do not limit the maximum mass flow but have lower efficiency and minimum mass flow may be limited by vaneless diffuser stall. Low Solidity Diffusers (LSD) are characterized by a small number of short vanes and do not show a well defined throat section. They intend to stabilize the flow at low mass flow without limiting the maximum mass flow by choking. The solidity (chord/pitch) is typically of the order of 1 or less (Fig. 23). A multipoint optimization is mandatory for the LSD design because achieving a wide operating range is the major target.

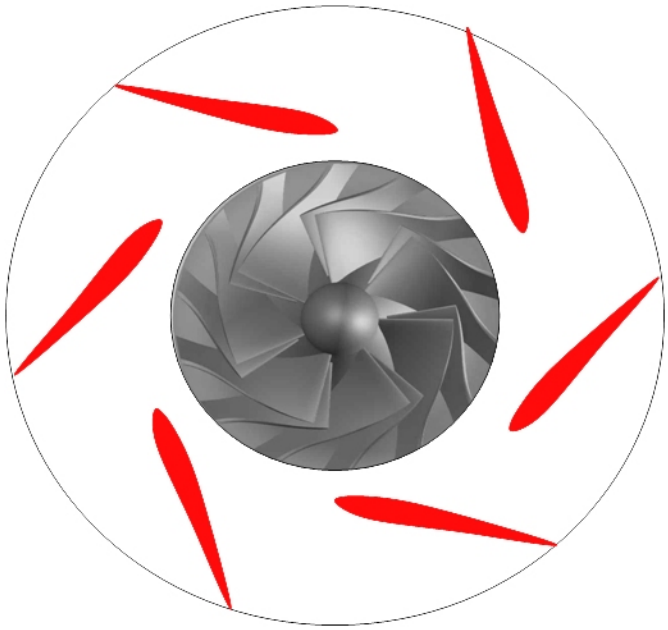

Fig. 23 Low Solidity Diffuser

The optimization of the LSD described here is done for the 3 operating points listed in Table 2 . Inlet conditions are different for each operating point because they result from a different operation point of the impeller. It is not possible to impose a pressure ratio corresponding to the impeller mass flow

because maximizing the diffuser design- and off-design pressure ratio is the target of the optimization process. Hence the mass flow will be different for every geometry. However it is expected that the performance at the low Mach number flow with fixed inlet angle will not noticeable be influenced by a modest change in mass flow.

Table 2 Diffuser inlet conditions at the 3 operating points

	surge	design	choke
A (flow angle)	62.5°	52.8 °	37.5 °
Mass flow	162.8	210.0	267.5

The blade geometry is defined by a NACA thickness distribution superposed on a camber line defined by a 4 parameter Bezier curve The 5th design parameter is a scale factor for the NACA thickness distribution (between .7 and 1.3). The 6th parameter is the number of blades (between 6 and 21). The last design parameter is the blade height. It is constant from leading edge to training edge but can be different for the prescribed impeller outlet width.

The main performance parameters are the static pressure rise- and total pressure loss coefficient

$$Cp = \frac{\overline{P}_3 - \overline{P}_2}{\overline{P}^o{}_2 - \overline{P}_2} \qquad \omega = \frac{\overline{P}^o{}_2 - \overline{P}^o{}_3}{\overline{P}^o{}_2 - \overline{P}_2}$$

They are calculated from the 3D Navier Stokes results obtained by means of the TRAF3D solver on a grid with 400 000. cells.

Making the Database is quite costly because it requires analyzing every geometry at three operating points. The initial Database is therefore limited to only 10 randomly generated samples requiring 30 Navier Stokes calculations.

The outlet over inlet pressure ratio defines the outlet boundary condition and cannot be used as an objective for the optimization. Losses only are also not sufficient to measure the performance because minimum losses may be obtained without any pressure rise. One wants to achieve the maximum pressure rise with minimum loss to keep the maximum kinetic energy available for the downstream components. Hence one must also consider the losses that are generated to reach that pressure rise.

The optimizer therefore aims to maximize following *OF*

$$OF = (1-(w_{low}.Cp_{low} + w_{mean}.Cp_{mean} + w_{high}.Cp_{high})) + w_{low}.\omega_{low} + w_{mean}.\omega_{mean} + w_{high}.\omega_{high}$$

This corresponds to a maximization of *Cp* while minimizing the losses. Taking into account that

$$Cp + \omega = Cp_{isentropic}$$

it is clear that minimizing the losses helps to reach the isentropic *Cp*. The latter is geometry dependent.

The outcome of the optimization is illustrated on Fig. 24. All diffusers show low losses with an increase of *Cp* at all operating points up to *Cp*+ω=.74. Higher values of the latter give rise to increasing losses and a decrease of *Cp* at low mass flow. Iteration 17 is considered as the optimum because of only a small decrease of *Cp* at minimum mass flow.

The Mach number distribution around the optimized vanes is shown on Fig. 25. One observes a small flow separation at minimum mass flow corresponding to the increase of the losses shown on Fig. 24.

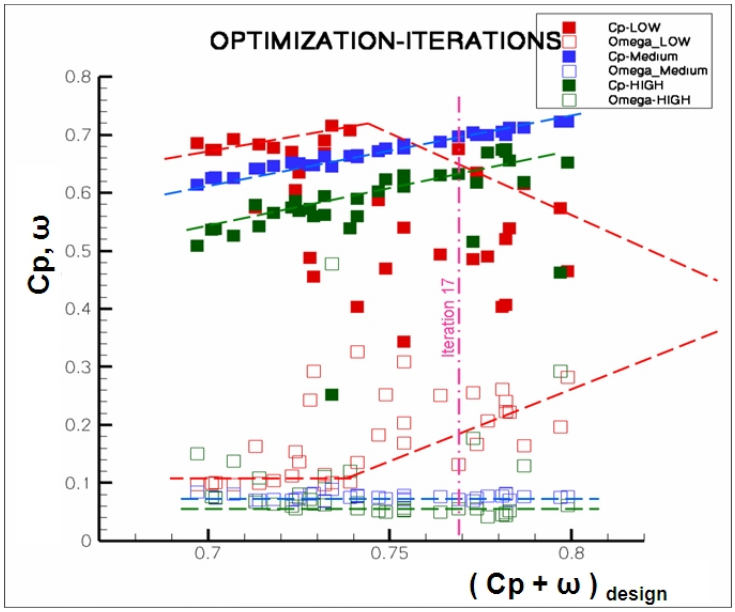

Fig. 24 Performance criteria of LSD

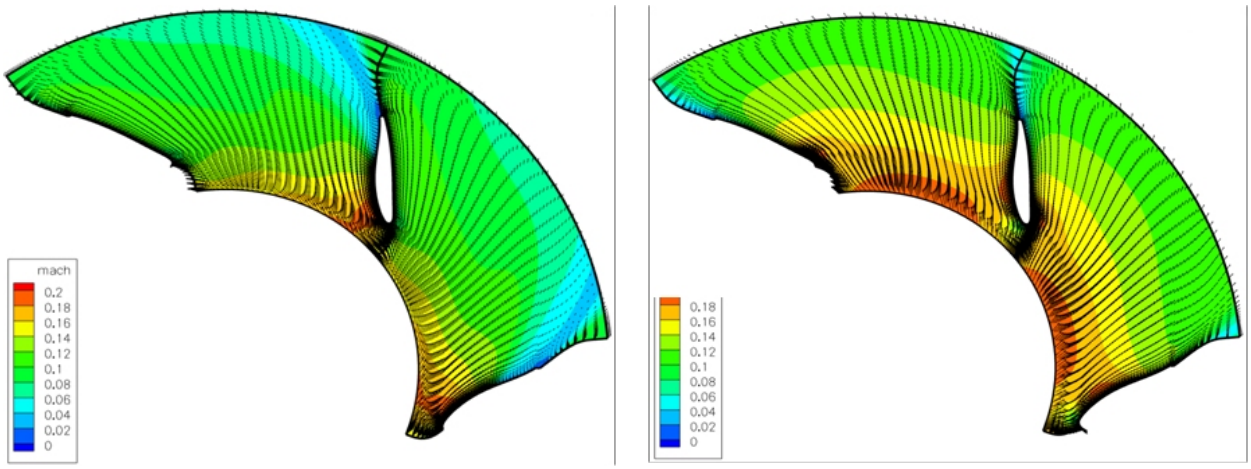

low $\dot{m}$ max $\dot{m}$

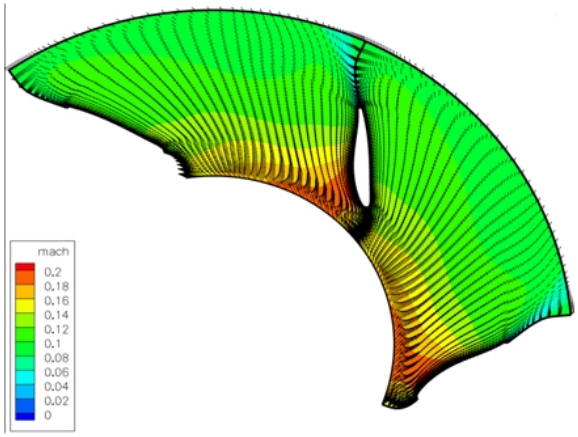

med $\dot{m}$

Fig. 25 Mach number distribution in the optimized geometry at the three operating points

6.2 Multipoint optimization of a radial compressor impeller

The mass flow in compressors is an outcome of a compressible flow calculation whereby the pressure ratio is imposed. Verifying if the target surge and choking mass flows are reached therefore requires knowing the corresponding pressure ratio before the calculation is made. The procedure developed at the VKI therefore calculates the flow at three predefined pressure ratios. A low one to find the choking mass flow, one corresponding to what is estimated the pressure ratio at design point and one at higher pressure ratio. This allows drawing a performance curve (indicated in bleu on Fig. 26) which is unlikely to satisfy the required choking mass flow. A simple scaling of the inlet section allows defining a new geometry that does satisfy this requirement. This first performance curve also allows a better definition of the design point pressure ratio. A last information is the pressure/mass flow slope allowing a guess of the pressure ratio at the required surge point mass flow. This is verified by an analysis of the scaled geometry and the resulting performance curve (red one) allows verifying if the targets are reached: i.e. choking mass flow, best efficiency at design mass flow and minimum pressure mass flow slope. A minimum of six flow analyses are required for each optimized geometry proposed by the GA.

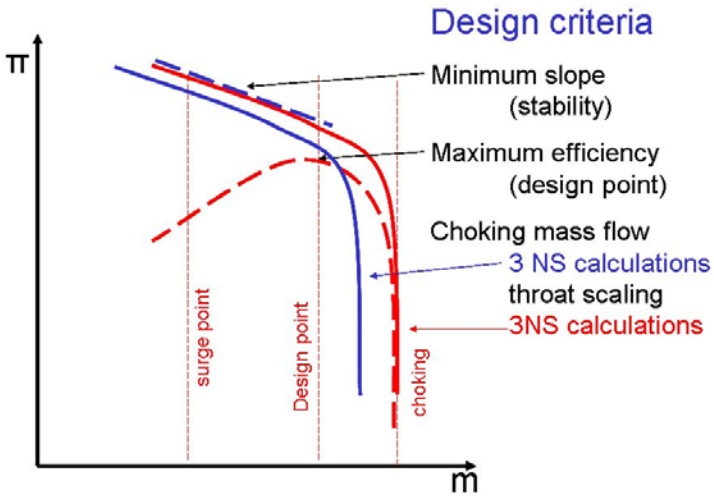

Fig. 26 Procedure for multipoint compressor optimization

7. MULTIOBJECTIVE OPTIMIZATION

7.1 Pseudo Objective Function versus Pareto front

Cooling HP turbine blades allows increasing the thermal efficiency by operating at higher Turbine Inlet Temperature (TIT) while maintaining the lifetime of the turbine. However the cooling air does not contribute to the work output and should be minimized because of its negative impact on thermal efficiency. Hence minimizing coolant flow and increasing lifetime are conflicting objectives. One way to satisfy both requirements, already explained in section 4.3, is by defining a pseudo *OF* that increases with insufficient lifetime and the amount of coolant mass flow.

$$OF(G) = w_l.P_l(G) + w_m.P_m(G)$$

The balance between the different objectives is defined by the respective weight factors. The task of the optimization algorithm thereby consists in finding the geometry that minimizes this pseudo *OF*.

However the balance between the different objectives may not be clear from the beginning. The different *OF* can then be plotted in the fitness space allowing a tradeoff between the two goals (Fig. 27). The non dominant solutions define a Pareto front. i.e. the collection of the geometries *G* for which one

objective cannot be decreased without increasing the other one. The choice is then left to the designer to select at the end of the optimization one geometry out of the non-dominated ones, that has the right balance between both objectives.

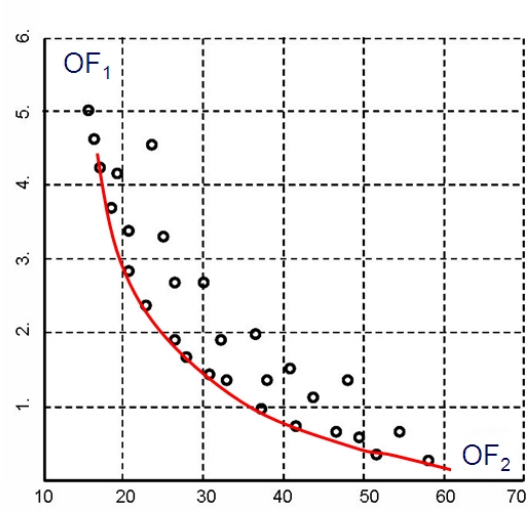

Fig. 27 Definition of Pareto front

The relation between the pseudo *OF* and the Pareto front approach is illustrated on Fig. 28. Optimization driven by a pseudo *OF* will follow a path in the direction of the red arrow on the figure; i.e. perpendicular to the slope defined by $OF(G) = w_l.P_l(G) + w_m.P_m(G)$. Convergence is reached when the line of constant *OF* is parallel to the Pareto front. The main advantage of using a pseudo *OF* is that fewer geometries need to be analyzed to find this optimum. The disadvantage is that the pseudo *OF* approach requires a rather good idea of the relative weights to be given to both penalties. The choice of the relative weights is rather obvious when one objective must be satisfied without compromise. This was the case when optimizing the radial compressor, shown in section 4, i.e. where the stress penalty had to be satisfied at all cost.

The advantages and disadvantages of both approaches are illustrated by the optimization of the cooling system of a HP turbine blade

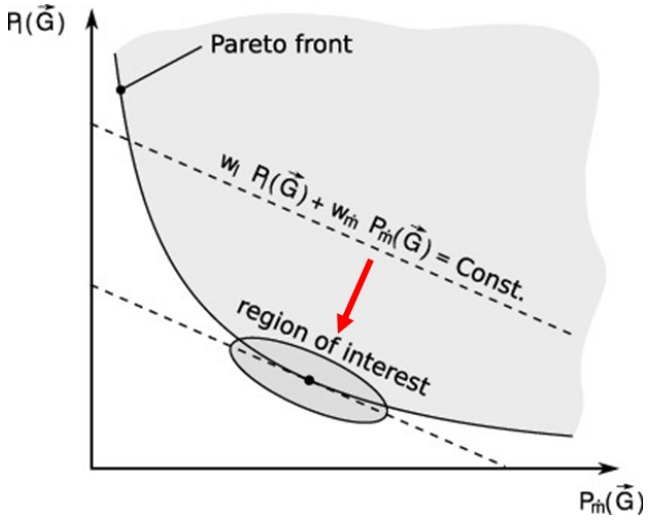

Fig. 28 Pseudo Objective Function versus Pareto front

7.2 Optimization of a cooled turbine blade

The optimization of an internal cooling system for an HP turbine aims for a reduction of the coolant flow while assuring the required lifetime. The mechanism is by uniformizing the metal temperature and in particular by limiting the metal temperatures in areas where the stresses are high [11].

Geometry parameterization

The cooling system to be optimized consists of five straight cylindrical channels. Design parameters are the position of their center at hub and shroud and their diameter. The centers are defined by the local curvilinear (η, ε) coordinates. The $\eta \in [0,1]$ coordinate represents the length along the camber line, while $\varepsilon \in [-1,1]$ defines the position perpendicular to the camber line (Fig. 29). The maximum value of ε (±1) corresponds to half the blade thickness at each η location. This facilitates the definition of a valid set of design parameters, i.e. for which the cooling channels do not intersect the blade wall. The local coordinates are the same at hub and shroud in order to reduce the number of design parameters.

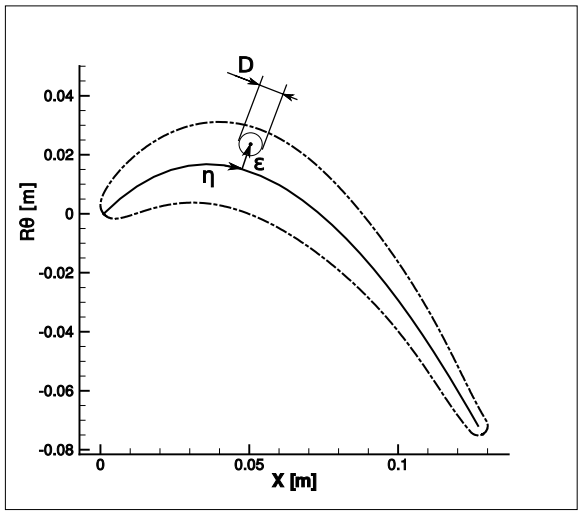

Fig. 29 Parameterization of the location and diameter of the cooling channel

Five individual cooling channels, parameterized by three numbers (η, ε and D), result in 15 design variables. Although the choice of relative coordinates reduces the number of invalid geometries, cooling channels can still be too close to the blade surface. Table 3 shows the individual range for all parameters of each cooling channel to avoid it.

Table 3 cooling hole parameter range

	η_{min}	η_{max}	ε_{min}	ε_{max}	D_{min}	D_{max}
cc1	0.050	0.225	-0.65	0.75	0.002	0.005
cc2	0.225	0.375	-0.60	0.75	0.002	0.006
cc3	0.375	0.600	-0.60	0.75	0.002	0.005
cc4	0.550	0.750	-0.60	0.70	0.002	0.005
cc5	0.700	0.950	-0.35	0.40	0.002	0.003

Lifetime Prediction

The prediction of the lifetime requires the calculation of the stresses and metal temperature inside the blade. The heat transfer from the external flow in the solid blade and cooling channel is calculated by a coupled method (CHT) [12]. It is a combination of a 3D NS solver for the external flow, a FEA method

for the internal heat transfer and stress calculation and a 1D non-adiabatic flow model for the cooling channel. Hence the method requires three grids (Fig. 30). Solid and fluid flow solvers alternate with an exchange of boundary conditions until the continuity of temperature and heat flux is obtained at their interfaces. The drawback of this approach is the need for sequential iterations between the two platforms and an interpolation of the boundary conditions from one grid to the other. The main advantage of the coupled approach is that one can make use of standard grid generators, NS and FEA solvers. Those codes have been extensively validated and their limitations and capabilities are well known. A FEA calculation is anyway needed to calculate the stresses.

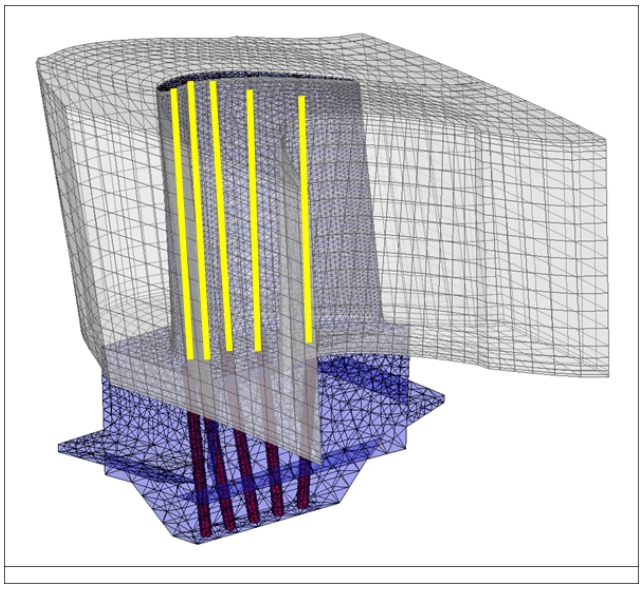

Fig. 30 Superposition of grids used in the coupled calculation

Upon completion of the heat transfer analysis, the solid temperature is known at each node of the FEA grid which allows a straight forward calculation of the thermal stress. The stresses due to the centrifugal forces and blade bending, resulting from the pressure difference between pressure and suction side, can be computed on the same grid with a temperature dependent material model. Assuming linearity, the total stresses are the sum of thermal, centrifugal and pressure stresses. Knowing the temperature and stress in each node of the FEA grid allows a computation of the blade lifetime.

The lifetime of the blade is assumed to be proportional to the creep-to-rupture failure according to Hill's anisotropic equation [13]. The equivalent stress γ ranges from 0 to 1. The material is considered to fail when γ= 1.

$$\gamma = H(\sigma_{xx} - \sigma_{yy})^2 + F(\sigma_{yy} - \sigma_{zz})^2 + G(\sigma_{zz} - \sigma_{xx})^2 + 2N(\tau_{xy})^2 + 2L(\tau_{yz})^2 + 2M(\tau_{zx})^2$$

H, *F*, *G*, *N*, *L* and *M* are material properties which depend on the Larson-Miller parameters in the longitudinal and transverse directions. They are specified by (Fig. 31)

$$LMP = T.[\log_{10}(l) + 23]$$

The parameters for the directionally solidified nickel superalloy material GTD-111 are used for the present analysis.

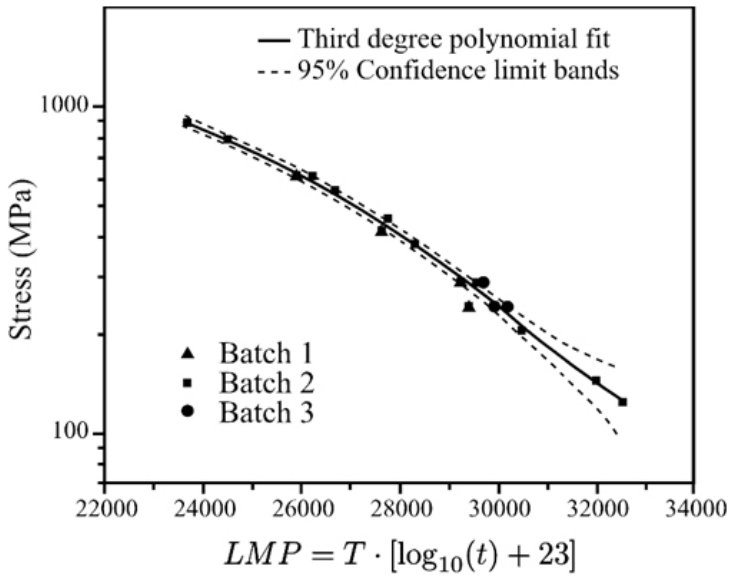

Fig. 31 Larson-Miller plot for longitudinal directional solidified GTD-111

The algorithm starts with a first guess of l and computes the Larson-Miller parameter in each node of the solid grid. These parameters are input for the calculation of the material properties (H, F, G, N, L and M). The material failure is checked in each node. Depending on the result, a new estimation of l is made, i.e. l is lowered if the maximum value of γ is larger than 1, or vice versa. This computation is repeated until a value of l is found for which the largest γ equals 1, plus or minus a tolerance.

Performance

The optimization method is the extension of the aerodynamic optimization tool for axial and radial impellers and stators and schematically shown on Fig. 12. The performance of the geometry is assessed after each CHT and thermal stress analysis or after the prediction by the metamodel. In order to achieve the target lifetime with the prescribed coolant mass flow, a penalty related to an insufficient lifetime and a too large coolant mass flow is given to each design. The task of the optimization algorithm thereby consists in finding the parameters that minimize the pseudo OF defined by

$$OF(G) = w_l.P_l(G) + w_m.P_m(G)$$

The penalty on the lifetime is proportional to the difference between the calculated $l(G)$ and target l_{tar} lifetime. The latter is set to 20000h, which is very high considering the high TIT(1400K) and the absence of a thermal barrier coating. This penalty is zero only if the target lifetime (l_{tar}) is exceeded (Fig. 32).

$$P_l(G) = \max(l_{tar} - l(G), 0.)$$

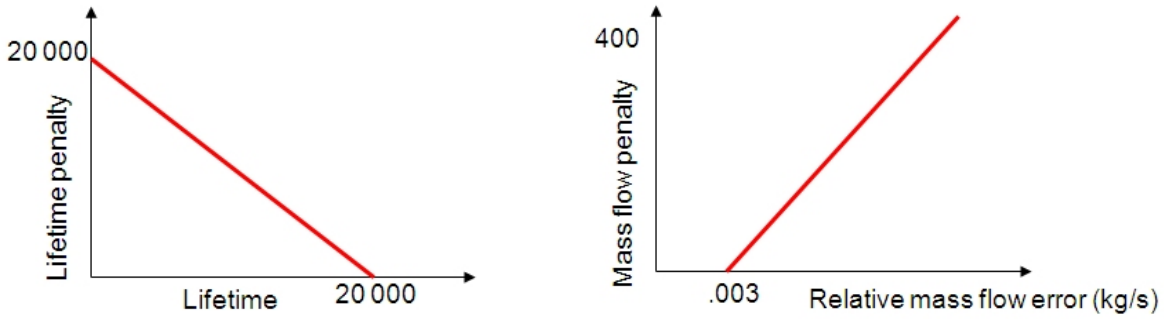

Fig 32 Lifetime and cooling mass flow penalties

A higher coolant mass flow results in a lower overall cycle efficiency and the penalty increases when the mass flow is higher than an offset value $\dot{m}_{offset} = 3gr/s$, as shown on Fig. 32.

$$P_m(G) = \max(\dot{m}(G) - \dot{m}_{offset}, 0)$$

Considering that the lifetime penalty is more important than the mass flow penalty, the weight given to the latter is 400. This results in a penalty of 133.33 for each g/s exceeding the limit of 3g/s. The weight given to the lifetime is 1/h.

Results

The starting geometry is a blade with 5 equidistant cooling holes. The surface temperature, von Mises and effective stresses are shown on Fig. 33. The lifetime based on thermal stresses of the cooled blade (220h) is hardly longer than the one of the uncooled blade (161h). The reason is that the solid temperature has decreased over most of the blade but not at the trailing edge hub where the largest stresses occur.

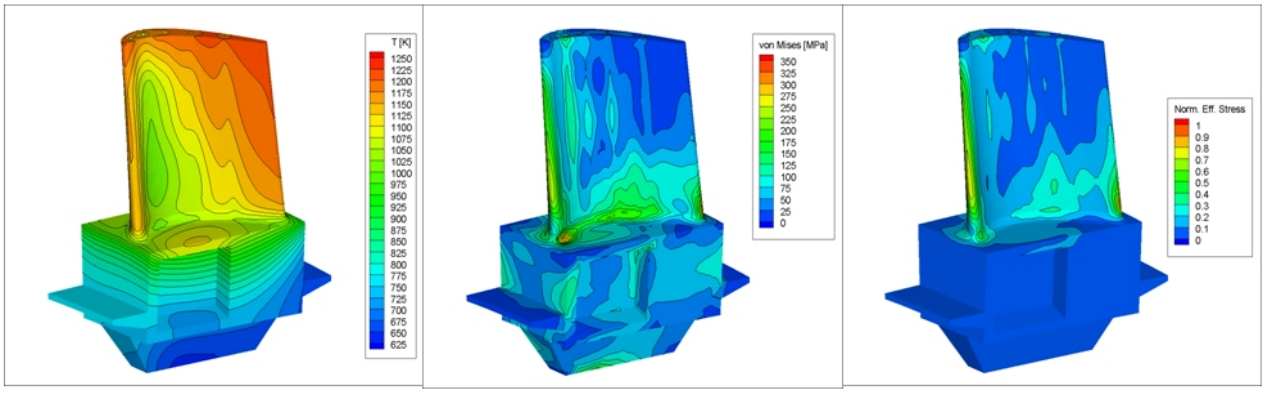

Fig. 33 Non optimized cooled blade (equidistant holes)

Two distinct optimizations are performed starting from the same initial database. One uses the ANN while the other one uses the RBF to predict the same quantities. Both optimizations are run for 30 iterations, after which a synchronization of the databases is made i.e. all existing samples are put together in one unified database. An additional 20 optimization iterations are then performed restarting with this extended database. The purpose of this synchronization is to exchange information between both optimizers and see if they can profit from it.

Fig. 34 shows, for both optimizations, the evolution per iteration of the mass flow, lifetime and total penalty. The metamodel predictions are compared with the results of the CHT and lifetime calculation. The mass flow in the individual cooling channels is immediately well predicted by the ANN whereas the method is too optimistic in terms of lifetime. The lifetime is better predicted by the RBF with a monotonic convergence towards the optimum except for 2 stepwise increases in lifetime. They correspond to a new choice by the optimization algorithm, based on the newly acquired information. It takes longer to accurately predicted the massflow by the RBF.

An increased discrepancy is observed after the synchronization of the databases at iteration 30. This is probably due to the larger number of training samples, requiring more hidden neurons, respectively RBF-centers to remain accurate. The best geometry proposed by the ANN is geometry 18. It has a total penalty of 14 058 corresponding to a lifetime of 6872h and a 10g/s cooling mass flow. The best RBF geometry is found at iteration 47 with a lifetime of 6758h for 10.4g/s cooling flow.

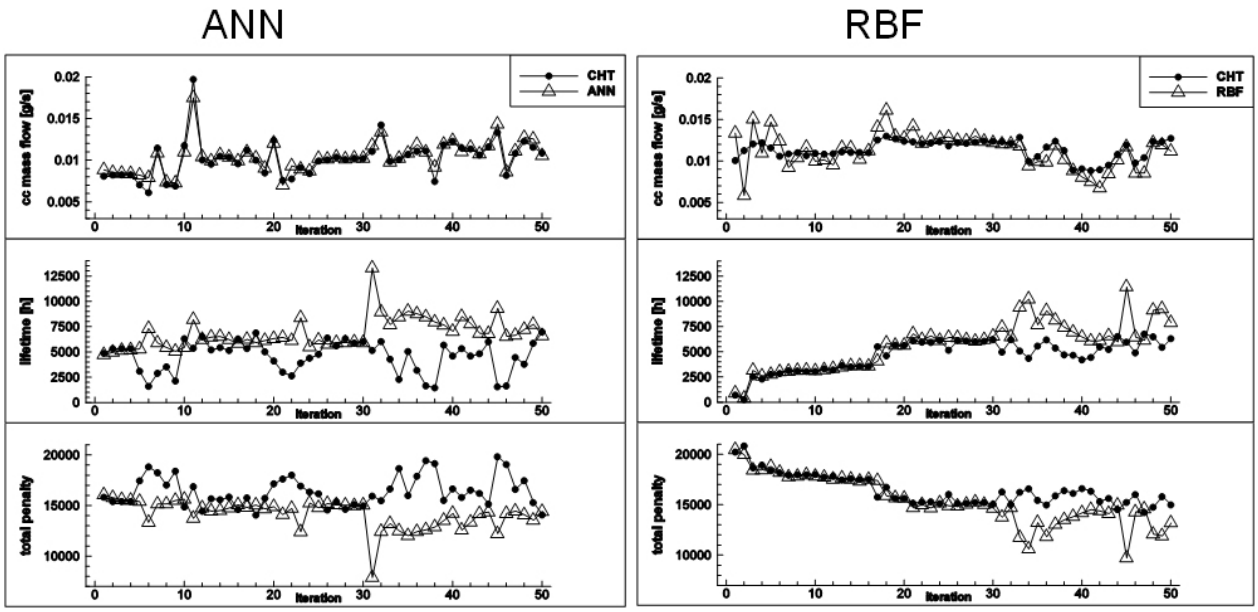

Fig. 34 Convergence with ANN and RBF

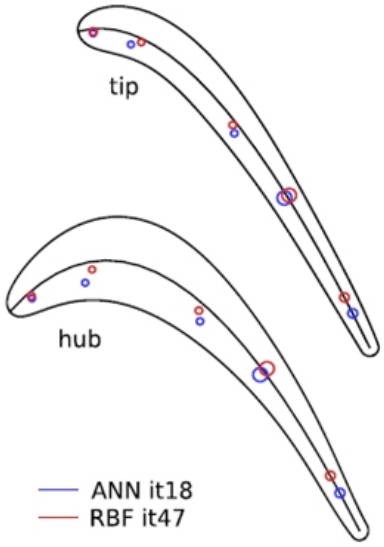

Fig. 35 Optimized cooling geometry

The optimal solutions found by both optimizations are compared on Fig. 35. A tendency towards small non-turbulated cooling channels, near the pressure side of the blade is observed. The trailing edge cooling channel should be positioned as far downstream as possible (h = 0.95). Hole number four has the largest diameter (4.4mm) with turbulators.

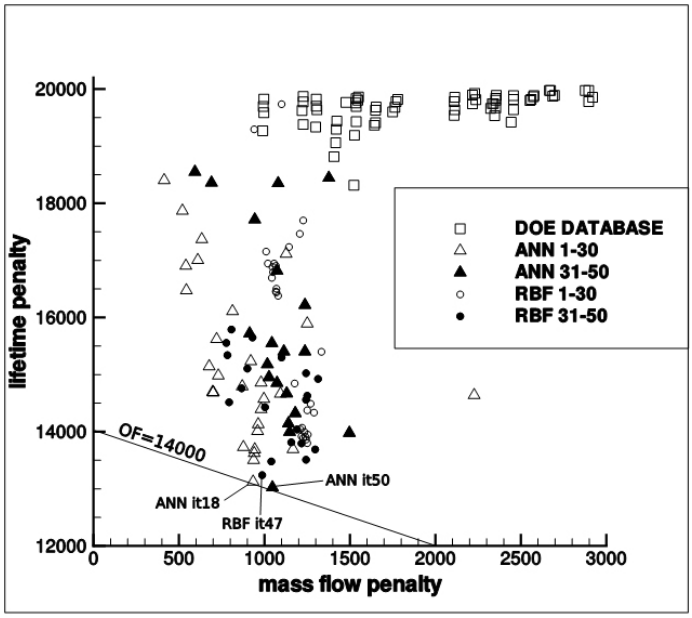

Fig. 36 Convergence to the optimum with pseudo *OF*

Figure 36 shows the mass flow penalty versus the lifetime penalty for the initial database samples and both optimizations. It is clear that all geometries created by the optimization system outperform the initial database ones. Whereas the maximum lifetime of the samples contained in the initial database does not exceed 1685h with an average lifetime of only 300h, most optimized geometries have a lifetime above 5000h. This illustrates the capability of the optimization system to rapidly improve the performance starting from only a limited information. The envelope of all the results form a Pareto front. It is a very incomplete one because the optimizer has been targeted towards a particular combination of the two penalty functions and a large part of the design space has not been investigated.

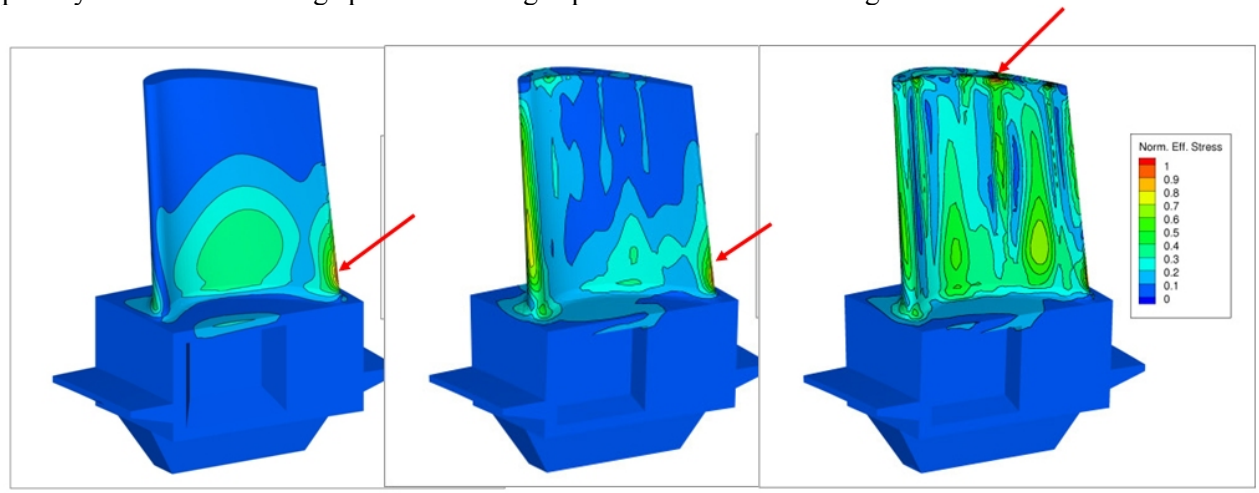

Fig. 37 Effective strength distribution at rupture

The effective stresses at failure on the surface of the uncooled (161h) , cooled (220h) and optimized (6872h) blade surface are shown on Fig. 37. The first two show no change in the critical area. The large improvement of the optimized one is the consequence of a more uniform stress distribution over the whole blade. The critical area has shifted from the hub trailing edge towards the blade tip. All parts of the blade are aging in almost the same

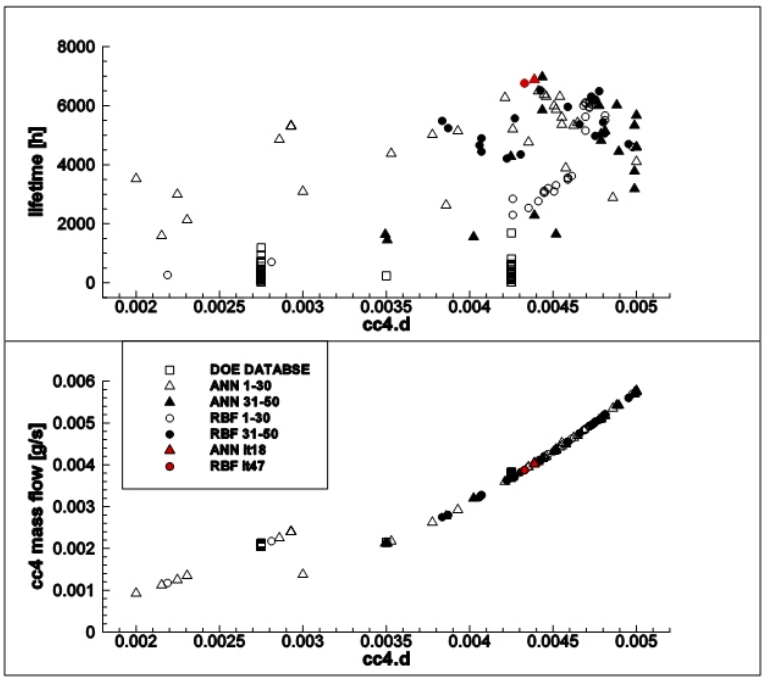

Fig. 38 Cooling channel 4 diameter versus lifetime and mass flow

Figure 38 shows the influence of the diameter of the 4th channel on lifetime and mass flow. A sudden variation in the mass flow is observed at 3mm due to the activation of the turbulators. The longest lifetime is obtained with a turbulated cooling channel of 4.4mm diameter. One also observes that the result is rather robust i.e. the lifetime does not change very much for small changes in the hole diameter.

7.3 Self Organizing Maps

The Pareto front is quite useful for problems with 2 objectives as long as it remains convex. A visualization becomes more complicated when 3 objectives are specified (Fig. 39).

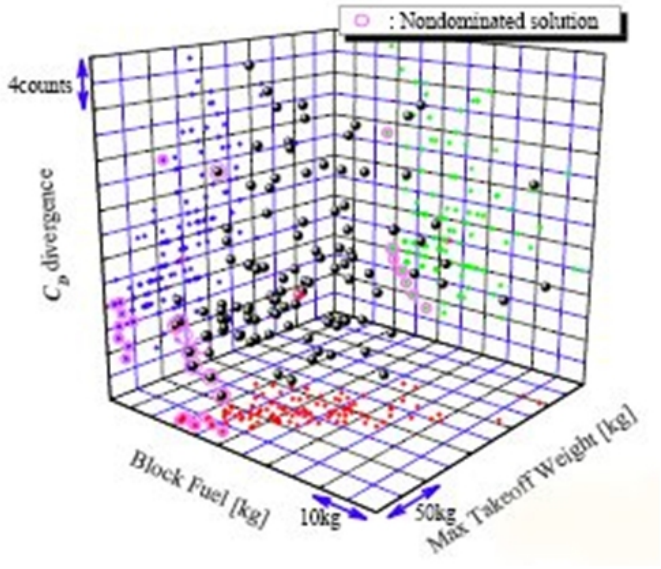

Fig. 39 Multi-objective Pareto front

Self Organizing Maps (SOM) [14] allow a balanced evaluation of the different geometries when more than three objectives are specified. The high dimensional maps are mapped into lower dimensional spaces by grouping geometries with similar characteristics.

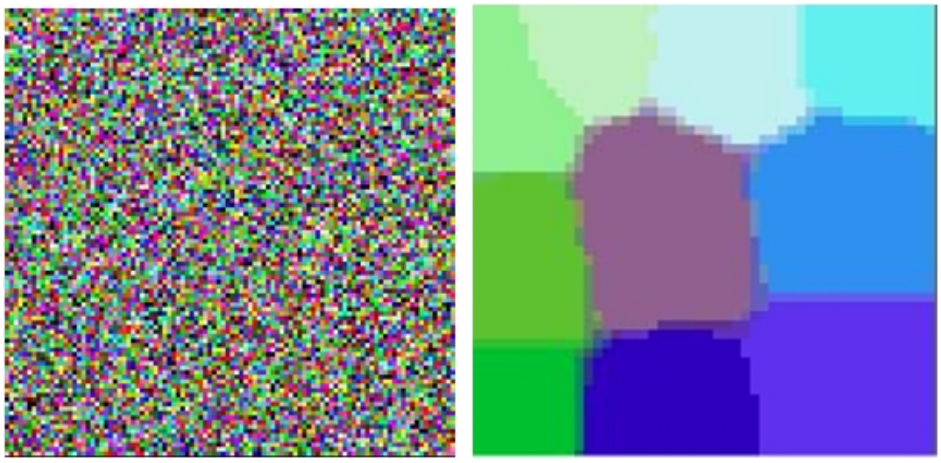

Fig. 40 Data mapping in organized maps

This is illustrated by the results of an airplane wing optimization where minimum drag at transonic and supersonic speed, bending and pitching moments are the four objectives to be reached. The different types of wing sections are grouped on Fig. 41. The corresponding values of the four objectives are shown by color on Fig. 42.

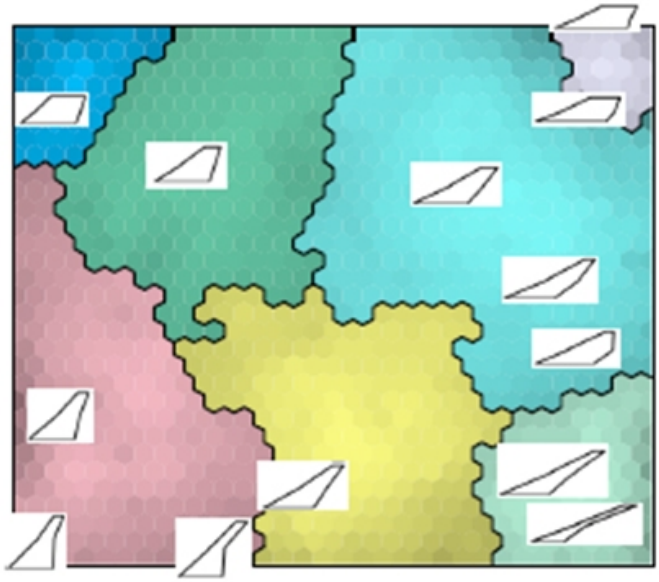

Fig. 41 Map of similar geometries

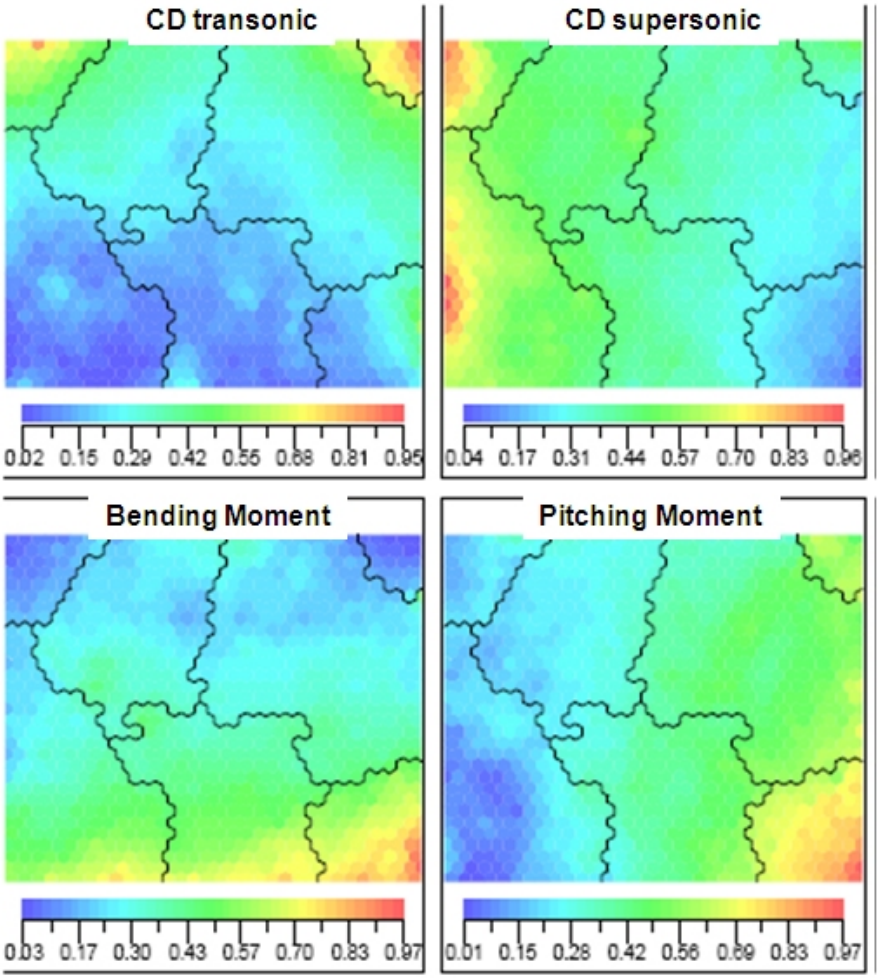

Fig. 42 Self organized maps

AKNOWLEDGMENTS

The contributions of Dr. S Pierret, Dr. T. Verstraete and Dr. Z Alsalihi are gratefully acknowledged.

BIBLIOGRAPHY

[1] Peter J., 2010. “Local optimization”, in: Strategies for Optimization and Automated Design of Gas Turbine Engines, RTO-MP-AVT-176, paper

[2] Aarts E.H.L. and Korst J.H.M., 1987, ``Simulated annealing in Boltzmann machines", Wiley Chichester.

[3] Bäck Th., 1996, ``Evolutionary Algorithms in Theory and Practice", Oxford University Press, N.Y.

[4] Rechenberg, I., 1973, “Evolutionsstrategie: Optimierung technischer Systeme nach Prinzipien der biologischen Evolution”, Stuttgart: Fromman-Holzboog.

[5] Van den Braembussche R.A., 2010. “Tuning of Optimization Strategies”, in: Strategies for Optimization and Automated Design of Gas Turbine Engines, RTO-MP-AVT-176, paper .

[6] Pierret S. and Van den Braembussche R.A., 1999, ``Turbomachinery Blading Design Using Navier Stokes Solver and Artificial Neural Network", ASME Journal of Turbomachinery, Vol. 121 pp. 326-332.

[7] Vanderplaats G.N., 1984, ``Numerical Optimization Techniques for Engineering Design", McGraw-Hill

[8] Arnone A., 1994, ``Viscous Analysis of Three-dimensional Rotor Flow Using a Multigrid Method", ASME Journal of Turbomachinery, Vol. 116, pp. 435-445.

[9] Verstraete T., Alsalihi Z. and Van den Braembussche R.A., 2007, ``Multidisciplinary Optimization of a Radial Compressor for Micro Gas Turbine Applications", ASME GT2007-27484.

[10] SAMCEF FEA code by: SAMTECH group, www.samcef.com .

[11] Verstraete, T., Amaral, S., Van den Braembussche, R. A., and Arts, T., 2008. “Design and Optimization of the Internal Cooling Channels of a HP Turbine Blade — Part II, Optimization”. In ASME. Paper No. GT2008-51080.

[12] Amaral, S., Verstraete, T., Van den Braembussche, R. A., and Arts, T., 2008. “Design and Optimization of the Internal Cooling Channels of a HP Turbine Blade — Part I, Methodology”. In ASME. Paper No. GT2008-51077.

[13] Dowling, N., 2007. *Mechanical Behaviors of Materials*. Prentice Hall.

[14] Sasaki S. and Obayashi S., 2004. “Adaptive Range Multi-objective Genetic Algorithm and Self Organizing Map for Multi-objective Optimization Problems”, in Optimization Methods for Multi-criteria/multidisciplinary Design Applications to Aeronautics and Turbomachinery, VKI-LS-2004-7